Journal Pre-proof

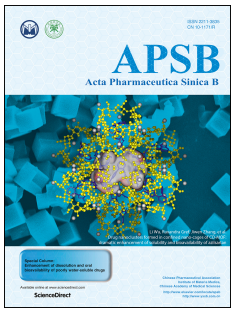

Obesity-driven oleoylcarnitine accumulation in tumor microenvironment promotes breast cancer metastasis-like phenotype

Chao Chen, Hongxia Zhang, Lingling Qi, Haoqi Lei, Xuefei Feng, Yingjie Chen, Yuanyuan Cheng, Defeng Pang, Jufeng Wan, Haiying Xu, Shifeng Cao, Baofeng Yang, Yan Zhang, Xin Zhao

PII: S2211-3835(25)00103-0

DOI: https://doi.org/10.1016/j.apsb.2025.02.026

Reference: APSB 2276

To appear in: *Acta Pharmaceutica Sinica B*

Received Date: 28 August 2024

Revised Date: 8 November 2024

Accepted Date: 20 December 2024

Please cite this article as: Chen C, Zhang H, Qi L, Lei H, Feng X, Chen Y, Cheng Y, Pang D, Wan J, Xu H, Cao S, Yang B, Zhang Y, Zhao X, Obesity-driven oleoylcarnitine accumulation in tumor microenvironment promotes breast cancer metastasis-like phenotype, *Acta Pharmaceutica Sinica B*, https://doi.org/10.1016/j.apsb.2025.02.026.

Original article

Obesity-driven oleoylcarnitine accumulation in tumor microenvironment promotes breast cancer metastasis-like phenotype

Chao Chen[a], Hongxia Zhang[a], Lingling Qi[a], Haoqi Lei[a], Xuefei Feng[a], Yingjie Chen[a], Yuanyuan Cheng[a], Defeng Pang[a], Jufeng Wan[a], Haiying Xu[a], Shifeng Cao[a], Baofeng Yang[a,b,*], Yan Zhang[a,c,*], Xin Zhao[a,*]

[a]*Department of Pharmacology, State Key Laboratory of Frigid Zone Cardiovascular Diseases (SKLFZCD), (State Key Labratoray-Province Key Laboratories of Biomedicine-Pharmaceutics of China, Key Laboratory of Cardiovascular Research, Ministry of Education), College of Pharmacy, Harbin Medical University, Harbin 150081, China*

[b]*Research Unit of Noninfectious Chronic Diseases in Frigid Zone, Chinese Academy of Medical Sciences, Harbin 150081, China*

[c]*Institute of Clinical Pharmacy, the Second Affiliated Hospital, Harbin Medical University, Harbin, Heilongjiang 150081, China*

Received 28 August 2024; received in revised 8 November 2024; accepted 20 December 2024

*Corresponding authors.

E-mail addresses: yangbf@ems.hrbmu.edu.cn (Baofeng Yang), zhangyan@ems.hrbmu.edu.cn (Yan Zhang), zhaoxin@hrbmu.edu.cn (Xin Zhao).

Running title: OLCarn promotes breast cancer cell EMT by ADCY10

Graphical abstract

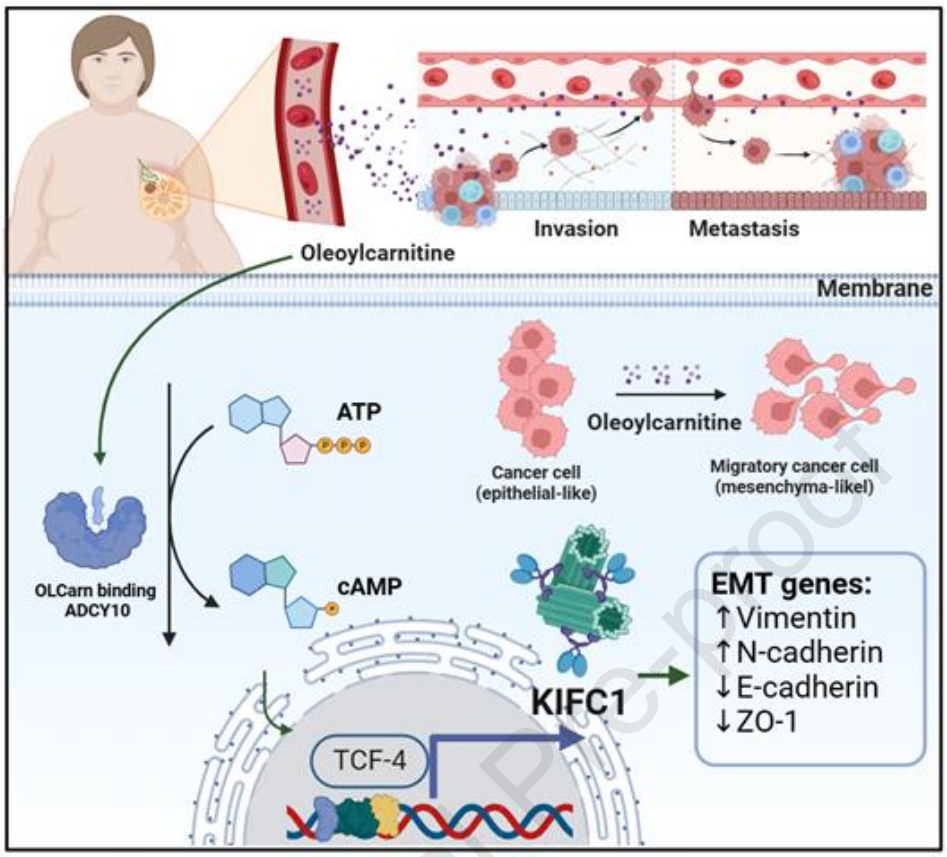

Circulating metabolite oleoylcarnitine, which accumulates due to obesity, promotes the metastatic phenotypic transformation of breast cancer.

Original article

Obesity-driven oleoylcarnitine accumulation in tumor microenvironment promotes breast cancer metastasis-like phenotype

Chao Chen[a], Hongxia Zhang[a], Lingling Qi[a], Haoqi Lei[a], Xuefei Feng[a], Yingjie Chen[a], Yuanyuan Cheng[a], Defeng Pang[a], Jufeng Wan[a], Haiying Xu[a], Shifeng Cao[a], Baofeng Yang[a,b,*], Yan Zhang[a,c,*], Xin Zhao[a,*]

[a]*Department of Pharmacology, State Key Laboratory of Frigid Zone Cardiovascular Diseases (SKLFZCD), (State Key Labratoray-Province Key Laboratories of Biomedicine-Pharmaceutics of China, Key Laboratory of Cardiovascular Research, Ministry of Education), College of Pharmacy, Harbin Medical University, Harbin 150081, China*

[b]*Research Unit of Noninfectious Chronic Diseases in Frigid Zone, Chinese Academy of Medical Sciences, Harbin 150081, China*

[c]*Institute of Clinical Pharmacy, the Second Affiliated Hospital, Harbin Medical University, Harbin 150081, China*

Received 28 August 2024; received in revised 8 November 2024; accepted 20 December 2024

*Corresponding authors.

E-mail addresses: yangbf@ems.hrbmu.edu.cn (Baofeng Yang), zhangyan@ems.hrbmu.edu.cn (Yan Zhang), zhaoxin@hrbmu.edu.cn (Xin Zhao).

Running title: OLCarn promotes breast cancer cell EMT by ADCY10

Abstract Obesity is a significant risk factor for cancer and is associated with breast cancer metastasis. Nevertheless, the mechanism by which alterations in systemic metabolism affect tumor microenvironment (TME) and consequently influence tumor metastasis remains inadequately understood. Herein, we found that perturbations in circulating metabolites induced by obesity promote metastasis-like phenotypes in breast cancer. Oleoylcarnitine (OLCarn) concentrations were elevated in the serum of obese mice and humans. Administration of exogenous OLCarn induces metastasis-like characteristics in breast cancer cells. Mechanistically, OLCarn directly interacts with the Arg176 site of adenylate cyclase 10 (ADCY10), leading to the activation of ADCY10 and enhancement of cAMP production. Mutations at Arg176 prevent OLCarn from binding to ADCY10, disrupting the ADCY10-mediated activation of cyclic

adenosine monophosphate (cAMP) signaling pathway. This activation promotes transcription factor 4 (TCF4)-dependent kinesin family member C1 (KIFC1) transcription, thereby driving breast cancer metastasis. Conversely, the neutralization of both ADCY10 and KIFC1 through knockdown or pharmacological inhibition abrogates the oncogenic effects mediated by OLCarn. Hence, obesity-induced systemic environmental changes lead to the aberrant accumulation of OLCarn within the TME, making it a potential therapeutic target and biomarker for breast cancer.

KEY WORDS Obesity; Breast cancer; Epithelial–mesenchymal transition; Metabolite; Oleoylcarnitine; ADCY10; KIFC1; cAMP

1. Introduction

Approximately 13% of cancers in women worldwide are attributed to obesity[1]. Obesity is a recognized risk factor for breast cancer; with each one-unit increase in body mass index (BMI), susceptibility to breast cancer increases by 8%[2]. Breast cancer patients who are overweight or obese have a 46% higher risk of developing distant metastases than those who are lean, and each 0.5-unit increase in BMI is linked to a 1.35 times higher risk of death from metastatic events[3]. However, the mechanisms underlying the relationship between obesity and the development of cancer remain unclear.

Emerging research indicates that obesity may expedite tumor progression by increasing the abundance of *Desulfovibrio* species in the intestinal microbiome, promoting cellular senescence, and impairing the function of macrophages and T cells. Studies on the relationship between obesity and cancer have predominantly focused on biological macromolecules such as senescence-associated secretory phenotype, mechanistic target of rapamycin, and programmed cell death protein 1[4-7]. However, there remains a significant gap in understanding how abnormal small-molecule metabolites, resulting from obesity-induced systemic metabolic alterations, influence the tumor microenvironment (TME).

Metabolic perturbations in nucleic acids, proteins, and other macromolecules can ultimately manifest as changes in small-molecule metabolites[8,9], which play pivotal

roles in tumorigenesis. For instance, 2-hydroxyglutarate[10], itaconate[11], fumarate[12], taurine[13], *β*-hydroxybutyric acid[14], and other small molecule metabolites have been demonstrated to be closely associated with the onset and progression of tumors. The level of methylmalonic acid, a byproduct of propionate metabolism, is elevated in the serum of older individuals, promoting SRY-Box transcription factor 4 expression and epithelial-mesenchymal transition (EMT)[15]. Oleoylcarnitine (OLCarn), a long-chain acylcarnitine, is synthesized through the esterification of dietary long-chain fatty acids, facilitates the transportation of fatty acids to mitochondria for energy production, and has been implicated in the progression of hepatocellular carcinoma (HCC)[16]. OLCarn concentration is also elevated in HCC, thereby serving as a potential biomarker[17]. However, the effect of OLCarn on the circulation in obese individuals with breast cancer metastases remains poorly understood.

Herein, we revealed that systemic environmental disturbances in obese individuals lead to the abnormal accumulation of OLCarn in the TME and drive breast cancer progression. Through metabolomics, we identified OLCarn, a metabolite that accumulates in the tumors and serum of obese mice, as a critical regulator of the EMT, invasion, and metastasis of breast cancer cells. Mechanistically, OLCarn serves as an activator of the adenylate cyclase 10 (ADCY10)-dependent cyclic adenosine monophosphate (cAMP/transcription factor 4 (TCF4) signaling pathway, upregulating the expression of (kinesin family member C1) KIFC1, and thereby promoting EMT in breast cancer. Moreover, obese individuals, whether diagnosed with breast cancer, exhibit significantly elevated serum levels of OLCarn, along with higher concentrations of OLCarn within their tumors. Hence, the high level of OLCarn in both the systemic environment and TME plays a pivotal role in breast cancer metastasis, making it a promising candidate as both a target and biomarker for breast cancer.

2. Materials and methods

2.1. Reagents and antibodies

For immunoblotting, antibodies were purchased from Cell Signaling Technology (anti-

E-cadherin, cat#14472S; anti-N-cadherin, cat#13116S), Bioss (anti-ZO-1, cat#bs-1329R; anti-*β*-actin, cat#bs-0061R), Immunoway (anti-Fibronectin, cat#YM3137; anti-PAI-1, cat#YT3569), Affinity Biosciences (anti-ADCY10, cat#DF13600), Santa Cruz (anti-Epcam, cat#K0320; anti-Vimentin, cat#E0721), ABconal (anti-ADCY10, cat#DF13600; anti-Snail, cat#A5243; anti-Slug, cat#A13352; anti-TCF4, cat#WH366135; anti-KIFC1 cat#WH299397; anti-GAPDH, cat#WH330321; anti DDDDK-Tag, cat#AE005), and Abcam (anti-TCF4, cat#ab217668). Secondary antibodies were procured from Beyotime (goat anti-rabbit Alexa Fluor 488, cat#A0423; goat anti-mouse Alexa Fluor 488, cat#A0428; goat anti-rabbit Cy-3, cat#A0516; goat anti-mouse Cy-3, cat#A0521), Sigma (streptavidin-Cy3, cat#S6402), and LI-COR (IRDye 800CW goat anti-rabbit, cat#926-32211; IRDye 800CW goat anti-mouse, cat#926-32210). Rhodamine-labeled ghost pen cyclic peptide (cat#CA1610) was obtained from Solarbio Science and Technology Co. Lipofectamine™ 3000 Reagent (cat#L3000-015) was purchased from Thermo Fisher Scientific. X-tremeGENE™ siRNA Transfection Reagent (cat#4476093001) was acquired from Roche. AZ82 (cat#1449578-65-7), LRE1 (cat#1252362-53-0), and IBMX (cat. #HY-12318) were procured from MedChemExpress. D-Luciferin sodium salt (cat#103404-75-7), p-cresol (cat#106-44-5), butanoic acid (cat#218926-46-6), phenylacetylglycine (cat#500-98-1), and OLCarn (cat#38677-66-6) were purchased from Aladdin, and stearylcarnitine (cat#25597-09-5) was purchased from Macklin. The lysis Buffer designed specifically for WB/IP assays was obtained from Absin (cat#abs9116). The cAMP ELISA detection kit (cat#BDEL-0401) was purchased from BioDragon.

2.2. Cell lines and treatment

Human and mouse breast cancer cell lines (HCC1806, MCF-7, and MDA-MB-231 E0771) and HEK-293T cells were purchased from the Cell Bank of the Shanghai Institute of Biochemistry and Cell Biology (Shanghai, China). MCF-7, MDA-MB-231, E0771, and HEK-293T cells were cultured in DMEM media (Gibco, USA), while HCC1806 cells were cultured in RPMI-1640 media (Gibco, USA). The culture medium

was supplemented with 10% fetal bovine serum (Meilun Bio, China) and 1% penicillin–streptomycin (HaiGene, China). The culture was maintained at 37 °C in a humidified atmosphere containing 5% CO_2 and 95% air. To treat with serum samples from high-fat diet (HFD) mice or obese patients, E0771 or HCC106 cells were incubated in culture medium containing 10% mouse or human serum for 3 days, following three PBS washes. To evaluate the potential effects of circulating metabolites in mice, HCC1806 cells were inoculated into standard culture medium with the addition of 5 or 10 μmol/L *p*-cresol, butanoic acid, phenylacetylglycine, stearylcarnitine, and OLCarn, or a vehicle (0.1% DMSO for phenylacetylglycine and OLCarn; double-distilled water for *p*-cresol, butanoic acid, stearylcarnitine).

2.3. Murine model and study design

All animal studies were approved by the Animal Ethics Committee of Harbin Medical University (Approval No. IRB5011723). Female C57BL/6 and BALB/c nude mice (4-8 weeks of age) were housed in specific pathogen-free or barrier conditions in animal facilities (Harbin Medical University, China). A cell-derived xenograft (CDX) model was constructed *via* subcutaneous injection of E0771 or HCC1806 cells (1×10^5 cells). In the orthotopic breast cancer models, tumors were induced in mice by injecting 1×10^5 HCC1806-luciferase cells suspended in 100 μL of a 1:1 mixture of PBS and Matrigel mixture into the fourth mammary fat pad on the right side of each mouse. For lung metastasis, 1×10^5 luciferase-expressing HCC1806 cells were injected into the tail veins of nude mice.

Following the establishment of these models, OLCarn was administered, and the tumors were surgically excised on Day 28. Thereafter, tumor metastasis was monitored for over 4 weeks. Primary tumors and metastases were monitored using a NightOWL II LB 983 system (Berthold, Germany).

2.4. Preparation of serum from C57BL/6 mice

The mice were randomly assigned to two dietary groups. Group 1 received a control

diet (cat# D12450B) with 10% fat, 20% protein, and 70% carbohydrates, while Group 2 was fed an HFD (Keao Xieli, China, cat# D12492) containing 60% fat, 20% protein, and 20% carbohydrates to induce obesity. The control diet was supplemented with 100% essential vitamins, minerals, amino acids, and fatty acids; detailed diet compositions have been provided in a previous study[18]. In Week 13, the mice were fasted for 10 h with access to water, after which blood samples were collected *via* cardiac puncture, allowed to clot for 30 min at room temperature and centrifuged at 1000 × *g* for 10 min.

2.5. Serum biochemical analysis

The levels of total cholesterol (TC, cat# H202), triglycerides (TG, cat#H201A), low-density lipoprotein cholesterol (LDL-C, cat#H207A), and blood glucose (cat#H108) were assessed using an automatic biochemical analyzer (Hitachi, Japan) and appropriate detection kits from the Medical System (Ningbo, China).

2.6. Delipidation and deproteinization in mouse serum

For the delipidation of mouse serum, Cleanascite Lipid Removal Reagent (BSG, USA) was employed following the manufacturer's protocol designed specifically for serum samples. A 1:4 volume ratio of Cleanascite reagent to the sample was utilized. To eliminate serum components larger than 3 kDa, a series of filtration steps was performed using size-exclusion columns. Initially, the serum was applied to ample prep centrifugal filter units (Milipore, USA) with a molecular size cut-off of 100 kDa and centrifuged at 4 °C and 4000 × *g*. The resulting flow-through fraction was subsequently processed consecutively using filter units with molecular size cut-offs of 50, 10, and 3 kDa. The delipidated serum fractions or size-excluded fractions of mouse serum were subsequently used in cell culture treatments, following the same procedures described for unprocessed mouse serum.

For deproteinization of mouse serum, the serum was meticulously transferred to an EP tube and subjected to vigorous vortexing and resuspension using pre-cooled 80% methanol to induce the denaturation and precipitation of all proteins. Subsequently,

centrifugation at 15,000 × *g* was performed at 4 °C for 20 min. The supernatant was freeze-dried and used as reserve culture medium.

2.7. Quasi-targeted metabolomic analysis of serum

Quasi-targeted metabolomic analyses were performed using Novogene (Tianjin, China). The serum pretreatment procedure was analogous to the deproteinization process. The resulting supernatant was then injected into the LC–MS/MS system for analysis.

2.8. Measurements of OLCarn concentrations in serum and tissue

Serum samples were subjected to direct vortexing and subsequent resuspension in pre-cooled 80% methanol, whereas tissue samples were ground and resuspended in 80% methanol to facilitate protein denaturation and precipitation. Following a 5 min incubation period on ice, centrifugation was performed at 15,000 × *g* at 4 °C for 20 min. Subsequently, an appropriate portion of the supernatant was diluted with double-distilled water until a 53% methanol concentration was obtained. The treated samples were then transferred to fresh EP tubes for another round of centrifugation under identical conditions. Finally, the supernatants prepared from the serum and tissue samples were analyzed using HPLC–MS.

2.9. Global gene expression analysis (RNA-seq)

RNA-seq was performed using Novogene (Tianjin, China). RNA from HCC1806 cells treated with 20 μmol/L OLCarn for 3 days was isolated *via* TRIzol method. RNA integrity was determined using an RNA Nano 6000 Assay Kit on a Bioanalyzer 2100 system (Agilent Technologies, USA).

2.10. Small interfering RNA and plasmid transfection

shKIFC1#1, shKIFC1#2, shADCY10#1, shADCY10#2, and shNC lentiviruses were purchased from GeneChem (Shanghai, China). KIFC1 or ADCY10 small interfering RNA (siRNA) were procured from Guangzhou RiboBio Co., Ltd. (Guangzhou, China).

Nonspecific siRNA was used as a negative control. Cells were transfected with siRNA using X-tremeGENE for 24 h according to the manufacturer's instructions. Plasmids containing wild-type *ADCY10* or the *ADCY10* Arg^{176} mutant were provided by Ubigen (Guangzhou, China). An empty *pcDNA3.1* vector was used as a negative control. These plasmids were transfected into HEK-293T cells for 24 h using Lipofectamin™ 3000, following the detailed instructions provided by the manufacturer.

2.11. Streptavidin–biotin affinity pull-down assay

Following synthesis of biotin-conjugated OLCarn, HCC1806 cells were lysed using a Lysis Buffer designed specifically for WB/IP assays (Absin, China). The prepared cell lysates were then incubated with either free biotin (20 μmol/L, MCE, USA) or biotin-OLCarn (20 μmol/L) for 12 h at 4 °C with continuous rotation. Subsequently, pre-washed streptavidin magnetic beads (MCE, China) were added to the system and incubated with gentle rotation at room temperature overnight. To remove non-specifically bound proteins, the beads were washed three times with elution buffer. The denatured proteins were then separated *via* SDS-PAGE and visualized with Coomassie blue staining. Differentially expressed proteins were identified using mass spectrometry conducted by SpecAlly (Wuhan, China).

2.12. Molecular docking

Molecular docking experiments were conducted using AutoDock4.2 software to assess direct interactions or binding between small molecules and proteins[19], whereas SiteMap software was utilized to predict the most favorable binding site for OLCarn[20]. The bicarbonate binding site in ADCY10 protein was used as a reference. The docking center was established based on the predicted binding site, with the coordinates X=20.01, Y=19.61, and Z=–0.04 serving as the center. To encompass the target area adequately, a cube with a side length of 22.5 Å was designated as the box size, and a spacing step of 0.375 was set. Genetic algorithm-based conformational sampling and scoring were employed, with a maximum limit of 10,000 conformations searched. A

flexible docking methodology was used, and the optimal conformation was selected based on the docking score for subsequent conformational sorting.

2.13. Drug affinity response target stability (DARTS) assay

After harvesting HCC1806 cell lysates through centrifugation, protein concentrations were determined using a BCA protein kit. Experimental protein solutions were diluted to a concentration of 1.5 g/L in M-PER buffer (Invitrogen, USA). Subsequently, the protein solutions were incubated with DMSO and 20 μmol/L OLCarn at room temperature for 2 h. The samples were pre-warmed in a metal bath at 40 °C for 10 min. Pronase E (Yuanye, China) PBS solution at a concentration of 5 mg/mL and an enzyme to protein ratio of 1:50 was added to each sample group. Samples were immediately digested in a metal bath at 40 °C for 20 min. Western blot analysis was performed to assess ADCY10 expression.

2.14. Cellular thermal shift assay (CETSA)

Cell lysates were prepared by adding RIPA lysate and centrifuging the samples. The lysates were then supplemented with DMSO and 20 μmol/L OLCarn and incubated at room temperature for 2 h. To assess the stability of the protein complex, the lysates were divided into six fractions and heated at 40, 45, 50, 55, 60, and 65 °C for 3 min. After heating, samples were centrifuged at 20,000×*g* for 15 min, and the supernatants were collected and mixed with SDS-PAGE loading buffer for Western blot analysis.

2.15. Intracellular co-localization of Bio-OLCarn and ADCY10

HCC1806 and HEK293T cells were pretreated according to the immunofluorescence assay protocol. The treated cells were subsequently incubated with anti-ADCY10 antibody (1:100) and Bio-OLCarn at a final concentration of 20 μmol/L or Biotin mixture overnight at 4 °C. Following primary antibody binding, the cells were exposed to goat anti-rabbit Alexa Fluor 488 secondary antibody (1:1000) and streptavidin-Cy3 (1:1000) in the dark for 1 h. Confocal microscopy was utilized to capture images, and

Image J software was employed for co-localization analysis of Bio-OLCarn and ADCY10 signals.

2.16. Intracellular cAMP measurement

The cells were pre-incubated for 24 h in culture medium free of sodium bicarbonate. The medium was then discarded, and the cells were treated with 0.5 mmol/L IBMX for 10 min. The cellular cAMP levels were quantified according to the manufacturer's instructions.

2.17. Three-dimensional (3D) tumor spheroid invasion assay

A 3D tumor spheroid invasion assay was performed following the designated protocol[21]. Breast cancer cells were detached using 0.25% trypsin, resuspended at a density of 10^4 cells/mL, and dispensed into ultra-low attachment 96-well round bottom plates (EFL, China) at a volume of 200 μL/well. Following 72 h of tumor sphere formation, 100 μL/well (50%) growth medium was removed and replaced with a 1:1 mixture of Matrigel Matrix (Corning, USA) and Rat Tail Collagen I (Corning, USA) in U-bottom wells. Subsequently, 100 μL/well of medium containing 30% CTD or HFD serum (final concentration 10%) was added. Phase-contrast microscopy was used to capture images at all time points. A minimum of four parallel experiments was conducted to obtain reliable results.

2.18. Transwell assay

To assess cancer cell invasion, E0771, HCC1806, and MCF-7 cells were stimulated and introduced into a matrix gel-coated chamber to enable their migration through membrane pores. After treatment, the invading cells were fixed in methanol for 10 min and rinsed three times with PBS. The membrane was stained with 0.5% crystal violet for 10 min, followed by three washes with PBS. Non-invasive cells on the upper membrane were removed, and the membrane was air-dried and photographed under a light microscope (Leica, Germany). The area of invasive cells was quantified using the

ImageJ software.

2.19. Histological evaluation and immunohistochemistry (IHC)

For histological examination, the tissue specimens were collected and fixed in 4% paraformaldehyde in PBS. Subsequently, they were embedded into paraffin blocks, sectioned to 4 μmol/L thickness, and stained with HE (Solarbio, cat#G1121) according to established protocols. Bright-field images were captured using an inverted microscope (Olympus BX43, Japan). For IHC analysis, the deparaffinized sections were incubated overnight at 4 °C with primary antibodies against E-cadherin (1:100), N-cadherin (1:200), KIFC1 (1:200), and TCF4 (1:200). Subsequently, the sections were incubated with species-specific secondary antibodies (1:1000). Confocal microscopy (Olympus FV10i, Japan) was used to capture images.

2.20. qRT-PCR

Tissue samples and cultured cells were subjected to RNA extraction utilizing the TRIzol reagent (Life Technologies, USA). Total RNA was quantified using a Nanodrop spectrophotometer (Thermo Fisher Scientific, USA), followed by reverse transcription to generate first-strand cDNA. SYBR Green real-time PCR was performed to determine gene expression levels in each sample. The primer sequences used in this study were as follows:

Human: KIFC1-F: (5′-AGCCTGAGAAGAAACGGACA-3′)

KIFC1-R: (5′-GATGGAACTCTTGGGTGGGA-3′)

GAPDH-F: (5′-CCACTCCTCCACCTTTGAC-3′)

GAPDH-F: (5′-ACCCTGTTGCTGTAGCCA-3′)

Mouse: KIFC1-F: (5′-AGGCCACCTTTGTTGGAAGTG-3′)

KIFC1-R: (5′-CCACGAGGTCCTGTCTTCTTAG-3′)

GAPDH-F: (5′-AATGGATTTGGACGCATTGGT-3′)

GAPDH-F: (5′-TTTGCACTGGTACGTGTTGAT-3′)

2.21. Chromatin immunoprecipitation (ChIP)

The ChIP assay was conducted employing a Pierce Magnetic ChIP Kit (Thermo Fisher Scientific, USA) according to the manufacturer's instructions. Briefly, cell lysates were sonicated to shear DNA into 200–500 bp fragments, and a ChIP-grade antibody targeting TCF4 was used for immunoprecipitation. The ChIP product was quantified through PCR using primers specific to the KIFC1 promoter. The following ChIP primers were used:

KIFC1-F: TGAGCAACAAGGAGTCCCAC

KIFC1-R: TCACTTCCTGTTGGCCTGAG

2.22. Western blot

Total cellular or tissue proteins were isolated using ice-cold RIPA buffer (Beyotime, China) with a protease inhibitor cocktail (Biosharp, China) and quantified using a BCA protein kit (Beyotime, China). Samples were analyzed through 10% or 12% SDS-PAGE, followed by transfer to nitrocellulose membranes (Millipore, USA). The membranes were blocked with TBST containing 5% skim milk for 1 h at room temperature. Primary antibodies were incubated overnight at 4 °C with gentle rocking, followed by secondary antibody incubation (Goat Anti-Rabbit or Mouse, 1:10,000) for 1 h at room temperature. Protein bands were visualized and analyzed using the Odyssey system (Li-COR, USA) to determine the gray values.

2.23. Human samples

The Ethics Board of Harbin Medical University approved the use of the human blood and tissue samples (Approval No. IRB5011723). Clinical data including sex, age, race, and BMI were collected from 28 healthy subjects without cancer (Supporting Informaiton Table S1). Informed consent was obtained from participants who were clinically diagnosed with breast cancer and underwent mastectomy. Cancerous or paracancerous tissues were obtained from 24 patients, and their clinical characteristics were documented (Supporting Informaiton Table S2). Tissues were fixed in 4%

paraformaldehyde or frozen in liquid nitrogen, while serum samples were stored in liquid nitrogen.

2.24. Quantification and statistical analysis

Statistical analyses were conducted using GraphPad Prism 9.0.2 software (GraphPad Software, USA). Data are presented as mean ± standard error of the mean (SEM). Student's *t*-test between two groups and one-way ANOVA across multiple groups were used to calculate *P* values. Pearson's correlation analysis was used to determine the correlation coefficient and *P*-values of BMI with OLCarn content. Statistical significance was determined based on a *P*-value threshold of less than 0.05 ($P<0.05$).

3. Results

3.1. Obesity accelerates breast tumor growth and metastasis

To establish a mouse obesity model, 5-week-old C57BL/6 mice were fed a control diet (10% kcal) or an HFD (60% kcal) for 13 weeks (Supporting Information Fig. S1A). Mice on an HFD showed significant weight gain and metabolic changes, including increased total cholesterol, triglyceride, and LDL-C levels, whereas fasting insulin levels remained similar between the groups (Fig. S1B–S1G).

Following dietary adaptation, syngeneic breast cancer cells (E0771) were used to create primary and lung metastatic tumor models (Fig. 1A). Consistent with previous findings[22,23], tumors of HFD-fed mice were significantly larger than those of control mice at the endpoint (Fig. 1B–E). In the lung metastasis model, HFD mice developed notable pulmonary nodules, unlike the smooth surfaces observed in the lungs of the control group (Fig. 1F and G). The number of nodules in the HFD group increased 2.5-fold compared to the control group (Fig. 1H).

The crucial role of EMT in promoting cancer metastasis is well-documented[24]. Our analysis revealed a significant reduction in epithelial markers (E-cadherin, ZO-1) and an increase in mesenchymal markers (N-cadherin, Vimentin) in the tumors of obese mice (Fig. 1I). Enhanced fluorescence of E-cadherin and N-cadherin confirmed the high

metastatic potential of these tumors (Fig. 1J–L). Additionally, *CDH1*, *EpCAM*, and *GATA3* expression decreased, whereas Serpine1 and Vimentin levels increased in obese mice, as shown in the GSE201316 dataset (Fig. 1M). These findings highlight the link between obesity and increased metastatic potential *via* the EMT in breast cancer.

Insert Fig. 1

3.2. Obesity-induced systemic environment promotes breast cancer aggression

Given the evidence that extrinsic factors in cancer cells significantly influence tumor progression, we postulated that obesity creates a systemic environment favorable for tumor advancement and aggressiveness. To test this hypothesis, we incubated E0771 cells with serum derived from CTD or HFD mice. The results indicated that E0771 cells treated with 10% serum of obese mice exhibited decreased levels of E-cadherin and EpCAM, along with increased levels of Vimentin, N-cadherin, Slug, and Snail (Fig. 2A and B). In contrast to the observed decrease in E-cadherin aggregation on the cell membrane, a significant increase in the membrane localization of N-cadherin was noted (Fig. 2C). Furthermore, the cytoskeletal structure became disorganized, which worsened the invasiveness of cancer cells (Fig. 2D and E).

To assess their metastatic potential, E0771 cells were treated with HFD serum and injected into the tail veins of athymic mice. Unlike CTD serum, HFD serum significantly enhanced the ability of cells to colonize the lungs and form metastatic lesions (Fig. 2F–H). In extended-duration 3D invasion assays, E0771 cell spheroids exposed to HFD serum showed a marked increase in invasion into adjacent matrices by Day 4, indicating that the cells underwent EMT before this time point, corroborating the EMT observed at 72 h (Fig. 2I and J).

Insert Fig. 2

3.3. Obese TME-derived OLCarn exacerbates breast cancer aggressiveness

The systemic environment, which is influenced by fats, proteins, and small molecules, plays a critical role in the TME. We investigated the serum components that induce

EMT in E0771 cells by removing proteins, fats, and molecules over 3 kDa. Notably, serum-deficient proteins and fats continued to induce EMT, highlighting the significance of small molecules (Supporting Information Fig. S2A and S2B).

To identify the key metabolites involved in EMT, we performed quasi-targeted metabolomics of mouse serum. Using partial least squares discrimination analysis, we detected 694 metabolites, of which 59 were upregulated and 124 were downregulated (Fig. S2C–S2E). These changes suggest that obesity reshapes circulatory and metabolic landscapes. We observed a 13-fold increase in p-cresol levels in the HFD serum, along with elevated levels of butyric acid, phenylacetylglycine, stearoylcarnitine, and OLCarn (Fig. 3A). Among these, only OLCarn induced a pro-aggressive EMT-like phenotype in E0771 cells, as evidenced by the decreased E-cadherin expression (Fig. S2F).

OLCarn, a long-chain acylcarnitine, serves as both an energy source and signaling molecule[25]. Large-scale exploratory metabolomic experiments often lack recognition because of their limited sensitivity and non-quantification[26]. We therefore quantified OLCarn in mouse serum and found significantly higher levels in HFD mice (391.2 ± 30.53 nmol/L) compared to CTD mice (285.5 ± 23.17 nmol/L) (Fig. 3B and C). Tumors of the HFD mice also showed increased OLCarn levels (Fig. 3D).

To assess the pro-aggressive effects of OLCarn, we treated E0771, triple-negative HCC1806, MDA-MB-231, and ER/PR-positive MCF-7 cells. At concentrations of ≥10 μmol/L, OLCarn upregulated the proteins associated with aggressiveness and induced an EMT-like phenotype (Fig. 3E, Supporting Information Fig. S3A–S3C). OLCarn-treated HCC1806 and MCF-7 cells displayed reduced E-cadherin levels, disorganized cytoskeletal structures, and increased invasiveness in both the 2D and 3D assays (Fig. 3F–H, Fig. S3D–S3H). In contrast, oleic acid and L-carnitine did not significantly affect EMT (Fig. S3I–S3K).

In vivo, OLCarn administration enhanced HCC1806 cell colonization in the lungs of athymic mice (Fig. 3I–K). Although OLCarn did not influence the growth of CDXs (Fig. S3L–S3O), it decreased E-cadherin and increased N-cadherin expression (Fig.

3L–M, Fig. S3P). In the orthotopic breast cancer model, OLCarn increased lung metastasis without affecting primary tumor growth (Fig. S3Q and S3R). Overall, these findings suggest that obesity-related changes in the systemic environment led to abnormal OLCarn accumulation in the TME, thereby promoting aggressive breast cancer characteristics.

Insert Fig. 3

3.4. KIFC1 mediates OLCarn-induced pro-aggressive phenotype reprogramming

To investigate the molecular mechanisms by which OLCarn facilitates cellular EMT, we performed RNA sequencing of HCC1806 cells treated with OLCarn for 3 days. The results demonstrated significant transcriptional reprogramming (Fig. 4A and Supporting Information Fig. S4A). Moreover, KEGG and GO analyses revealed enrichment in pathways associated with cell motility and adhesion, including gap junctions, tight junctions, and cell adhesion molecules, which are vital for EMT (Fig. 4B and C). Notably, we observed a reduced expression of the epithelial marker *TJP1* and alterations in other adhesion factors such as *CDHR5*[27] and *CD34*[28] following OLCarn treatment (Fig. 4D). These findings suggest that OLCarn modulates multiple signaling pathways involved in reshaping tumor cell adaptability to enhance EMT and invasiveness.

Among the differentially expressed genes, *KIFC1* emerged as a crucial player in EMT regulation[29-31]. High *KIFC1* expression correlated with poor overall survival in both lymph node-negative and lymph node-positive breast cancer cases (Fig. S4B and S4C), which led us to hypothesize that OLCarn modulates EMT *via* KIFC1. We analyzed the *KIFC1* mRNA and protein levels in HCC1806, MCF-7, E0771, and MDA-MB-231 cells treated with OLCarn and observed a concentration-dependent increase in KIFC1 expression (Fig. 4E and F, Fig. S4D–S4G). Furthermore, KIFC1 levels were significantly elevated in E0771 cells in response to the HFD serum compared to the CTD serum (Fig. S4H and S4I), and KIFC1 fluorescence intensity increased in syngeneic tumors from HFD mice (Fig. 1K).

Silencing KIFC1 *via* siRNA negated the effects of OLCarn on EMT and aggressive markers in HCC1806 and MCF-7 cells (Fig. 4G and H). Additionally, KIFC1 ablation blocked the ability of HFD serum to induce EMT markers in E0771 cells (Fig. 4I) and restored the cytoskeletal integrity disrupted by OLCarn under both 2D and 3D conditions (Fig. 4J–N, Fig. S4J–S4N).

To confirm that KIFC1 mediates OLCarn-induced EMT *in vivo*, KIFC1 knockdown HCC1806 cells were injected into nude mice. *In vivo* imaging and HE staining revealed that KIFC1 suppression inhibited OLCarn-induced lung metastasis and reduced the number of lung nodules (Fig. 4O–Q). Notably, OLCarn did not affect the size or weight of CDX tumors derived from KIFC1-deficient cells (Fig. S4O–S4Q) or the expression of E-cadherin and N-cadherin (Fig. 4R).

We also utilized AZ82, a specific KIFC1 inhibitor[32,33]; treatment with 1 μmol/L AZ82 effectively downregulated KIFC1 in HCC1806 and MCF-7 cells, reversing OLCarn-induced EMT, cytoskeletal disorganization, and increased invasiveness (Supporting Information Fig. S5A–S5G). These findings underscore KIFC1's critical role in mediating OLCarn-induced EMT and breast cancer metastasis.

Insert Fig. 4

3.5. OLCarn directly activates ADCY10 by binding to Arg176 site

To investigate how OLCarn upregulates KIFC1 expression, we performed a streptavidin-biotin affinity pull-down assay using biotin-conjugated OLCarn (Bio-OLCarn) and confirmed its ability (Fig. 5A and Supporting Information Fig. S6A). Mass spectrometry analysis identified 11 candidate proteins (Fig. 5B and C, Fig. S6B), including ADCY10, which catalyzes the conversion of ATP to cAMP and is associated with the cAMP signaling pathway (Fig. 4B and C)[34]. Although *ADCY10* expression did not correlate with overall survival in breast cancer, high *ADCY10* levels were associated with poorer outcomes in patients with lymph node metastasis (Fig. S6C and S6D), suggesting a role in metastasis. This indicates that ADCY10 may be involved in EMT and metastasis of breast cancer.

Therefore, we hypothesized that ADCY10 is crucial for OLCarn-mediated KIFC1 expression and EMT. To validate this, we examined the interaction between OLCarn and ADCY10 using Western blot analysis. Bio-OLCarn successfully precipitated ADCY10 from HCC1806 cell lysates (Fig. 5D), and co-localization analysis revealed a correlation coefficient of ~0.8 (Fig. 5E). These results suggested that ADCY10 is a direct target of OLCarn, as supported by subsequent DARTS[35] and CETSA[36] assays. Notably, Pronase E treatment significantly decreased ADCY10 levels; however, co-incubation with OLCarn elevated ADCY10 stability against proteolysis (Fig. 5F). OLCarn also shifted the ADCY10 melting curve to the right in thermal gradient assays, indicating enhanced stability (Fig. 5G).

To further explore this interaction, molecular docking analysis revealed that OLCarn's hydrophobic side chains interact with ADCY10's hydrophobic regions, with the carboxylic acid partially embedded and forming a hydrogen bond with Arg^{176} (the binding site for the ADCY10 agonist bicarbonate) at 2.9 Å. Additional interactions involved Phe336, Met337, Phe338, Phe45, and Met419 *via* hydrogen bonds and van der Waals forces (Fig. 5H). We assessed the agonistic effects of OLCarn in ADCY10 cells. While OLCarn did not alter ADCY10 expression (Fig. 5I and J), it significantly increased cAMP levels in HCC1806 and MCF-7 cells (Fig. 5K and L). Additionally, serum from HFD mice led to a two-fold increase in cAMP levels (Fig. 5M).

Next, we created a plasmid with a mutation at site 176 by substituting Arg with Gly ($ADCY10^{R176}$) and transfected this plasmid into HEK-293T cells (Fig. 5N and Fig. S6E). A pull-down assay demonstrated that OLCarn failed to bind to $ADCY10^{R176}$ (Fig. 5O). Although elevated cAMP levels were inadequate to elucidate the binding between OLCarn and ADCY10, as Arg^{176} is the binding site for bicarbonate (Fig. 5P)[37], CETSA (Fig. 5Q) and DARTS assays (Fig. 5R) indicated that OLCarn binding significantly stabilized $ADCY10^{WT}$ compared to $ADCY10^{R176}$. Thus, our findings suggested that OLCarn interacts with Arg176 in ADCY10.

Insert Fig. 5

3.6. OLCarn induces KIFC1 through activation of ADCY10/cAMP signaling

ADCY10 functions as a unique intranuclear source of cAMP and regulates various physiological processes, including transcriptional activity[38,39]. The knockdown of ADCY10 or treatment with the inhibitor LRE1[40] abolished the capacity of OLCarn to elevate cAMP levels in HCC1806 and MCF-7 cells (Fig. 6A and B, Supporting Information Fig. S7A and S7B). This inhibition also reduced OLCarn- and obese serum-induced KIFC1 expression, thereby disrupting the EMT, cell invasion, and cytoskeletal integrity (Fig. 6C–J, Fig. S6F–S6J and Fig. S7C–S7I).

Furthermore, ADCY10 deficiency impaired HCC1806 cell dissemination and colony formation in the lungs of athymic mice after OLCarn treatment (Fig. 6K–M). Similar to KIFC1 inhibition, ADCY10 knockdown suppressed tumor growth in CDXs treated with OLCarn (Fig. S6K–S6M)—a trend also observed in orthotopic breast cancer models (Supporting Informatin Fig. S7J and S7K). Additionally, ADCY10 deficiency reduced the regulatory effects of OLCarn on KIFC1 and EMT markers in the CDXs (Fig. 6N and Fig. S6N).

Moreover, TCF4, a transcription factor specific for KIFC1, is activated by ADCY10-PKA-mediated phosphorylation[41,42]. We observed significantly elevated TCF4 levels in the tumors of the obese and OLCarn-treated mice (Fig. 1K, Fig. 3M). Although ChIP-PCR demonstrated an increase in the level of the KIFC1 promoter sequence after the addition of OLCarn, it did not facilitate the binding of TCF4 (Fig. S7L). Inhibition of ADCY10 also abrogated the promoting effect of OLCarn on TCF4 expression (Fig. 6C–E, Fig. S7G and S7H). Collectively, OLCarn induced KIFC1 expression *via* the ADCY10/cAMP/TCF4 pathway.

Insert Fig. 6

3.7. OLCarn correlated with metastatic-like properties as a risk factor for breast cancer

To investigate the role of OLCarn in clinical samples, we compared serum OLCarn levels in subjects with normal weight (BMI 18–24) and obesity (BMI > 28). The mean OLCarn concentration was significantly higher in the obese cohort (35.67 ± 3.30

nmol/L) compared to the normal weight group (21.83 ± 1.40 nmol/L), with a correlation coefficient of 0.54 (95% CI) (Fig. 7A and B). Notably, HCC1806 cells exposed to serum obtained from obese subjects exhibited significant EMT (Fig. 7C). In non-obese breast cancer patients, serum OLCarn levels averaged 34.90 ± 4.23 nmol/L, while obese patients had levels as high as 59.13 ± 10.09 nmol/L, validating the positive correlation between BMI and OLCarn concentration (Fig. 7D and E).

We also assessed OLCarn levels in tumors and adjacent tissues of breast cancer patients. While no significant differences were found in adjacent tissues, tumor tissues of obese patients showed markedly higher OLCarn levels than those of normal-weight subjects (Fig. 7F). A positive correlation between BMI and OLCarn content in tumors was observed, with no such associated was noted in adjacent tissues (Fig. 7G and H). mIHC staining revealed decreased E-cadherin expression and increased fluorescence intensities of N-cadherin, KIFC1, and TCF4 in the tumors of obese patients (Fig. 7I and J). These results indicate that elevated serum OLCarn levels correlate with obesity, positioning OLCarn as a potential risk factor for metastasis in obese patients with breast cancer (Fig. 7K).

Insert Fig. 7

4. Discussion

Overweight and obesity significantly increase the risk of various diseases, including cardiovascular diseases, metabolic syndrome, and cancers[43,44]. Weight loss *via* a low-fat diet can inhibit tumor growth in murine models, whereas anti-obesity drugs such as semaglutide reduce body weight without affecting tumor progression[7]. Notably, some studies suggest that mild obesity may be linked to lower mortality and better survival in cancer patients, a phenomenon termed the “obesity paradox”[45]. This paradox may arise from the dual role of obesity in promoting cancer progression and enhancing immunotherapy response. Thus, obesity-induced systemic environmental remodeling is critical for tumor development.

Systemic environmental remodeling refers to alterations in the systemic circulation.

In our study, serum derived from mice subjected to an HFD was observed to facilitate breast cancer metastasis, independently of macromolecular components and fats, suggesting a possible association with small-molecule metabolites. Metabolomic analysis demonstrated that the serum metabolic profile of obese mice was altered, with an abnormal accumulation of OLCarn in the TME, which in turn promoted EMT and metastasis.

The exact mechanism of OLCarn production remains unclear but is believed to arise from an initial reaction between long-chain fatty acids and carnitine, catalyzed by carnitine palmitoyltransferase I (CPT1). This is followed by translocation across the mitochondrial membrane *via* carnitine-acylcarnitine translocase, where CPT2 regenerates acylcarnitine CoA[46]. Downregulation of CPT2 hampers fatty acid *β*-oxidation, leading to the accumulation of acylcarnitines, including OLCarn, which may promote malignant progression in HCC[16]. A prospective cohort study found a positive correlation between OLCarn levels in feces and obesity, consistent with our observations of elevated serum OLCarn levels in obese mice and humans[47]. Notably, we observed a 1.7-fold increase in serum OLCarn levels in obese patients with breast cancer compared with their non-obese counterparts. Interestingly, OLCarn levels were significantly lower in the serum than in tumor tissues, suggesting that it is produced in tumor cells or released by normal cells into the circulation for tumor uptake.

EMT is pivotal for tumor progression. Our study revealed that OLCarn induced dose-dependent EMT in various breast cancer cell lines. RNA-seq analysis revealed a significant increase in *KIFC1* expression in OLCarn-treated HCC1806 cells. Elevated *KIFC1* levels correlate with tumor recurrence, drug resistance, and metastasis, which adversely affect patient survival. KIFC1 stabilizes multiple centrosomes, enhances cell viability and polarity, remodels the cytoskeleton, and promotes EMT and metastasis[48]. We found that OLCarn upregulated KIFC1 at both the mRNA and protein levels, which may explain the increased KIFC1 expression in breast cancer tissues of obese patients. Notably, KIFC1 deficiency attenuated OLCarn- and obese-serum-induced EMT and metastasis *in vivo*, highlighting its role in mediating the effects of OLCarn.

To explore how OLCarn enhances KIFC1 expression, we identified ADCY10 as a key mediator using streptavidin–biotin pull-down assays and confirmed the co-localization of ADCY10 and OLCarn *via* immunofluorescence. Unlike transmembrane adenylate cyclases, ADCY10 is a soluble adenylate cyclase that remains inactive because of the salt bridge between Arg176 and Asp99. The binding of bicarbonate to Arg176 disrupts this bridge, activating ADCY10 to convert ATP to cAMP[49]. This mechanism likely facilitates the direct activation of ADCY10 by OLCarn, thereby promoting *KIFC1* expression and subsequent EMT.

Our findings indicated that OLCarn does not alter ADCY10 protein levels but binds to the Arg176 site, directly activating ADCY10 and promoting cAMP production. Notably, the Arg^{176} site serves as a binding site for bicarbonates. Given the low-pH of TME[50], which is characterized by the absence of bicarbonate, potential substitution of bicarbonate with OLCarn may be required to facilitate the phenotypic transformation of tumors. These findings suggested that ADCY10 is a specific protein target of OLCarn.

Because of the extensive cytoplasmic distribution of ADCY10, ADCY10–cAMP assumes diverse functional roles across various cellular compartments, including the nucleus. ADCY10 has been recognized as a distinctive source of cAMP within the nucleus, which regulates CREB activity in a PKA-dependent manner. Similarly, ADCY10–PKA-dependent phosphorylation and the subsequent activation of TCF4 are essential for brain development[42]. ChIP-PCR experiments demonstrated that OLCarn selectively enhanced *KIFC1* transcription without altering the binding affinity of its transcription factor, TCF4. This finding suggests that OLCarn can upregulate the expression levels of TCF4 but does not influence its transcriptional activity. Therefore, the precise mechanism by which OLCarn upregulates TCF4 *via* the ADCY10–cAMP signaling axis remains unclear.

Although further comprehensive investigations are warranted to fully elucidate the relationship between obesity and tumorigenesis, our study provides partial evidence that the remodeling of the serum metabolic profile induced by obesity significantly contributes to the progression of breast cancer.

5. Conclusions

The altered serum metabolic profile in obese individuals may contribute to the promotion of EMT and metastasis in breast cancer, and, more specifically, obesity can induce systemic environmental changes, leading to abnormal accumulation of OLCarn in the TME. Mechanistically, OLCarn serves as a signaling molecule that directly binds to ADCY10, activates the cAMP signaling pathway, and upregulates the expression of KIFC1 through TCF4, thereby promoting EMT and the metastatic potential of breast cancer. Therefore, OLCarn in both the systemic environment and the TME plays a pivotal role in breast cancer metastasis, making it a promising candidate as both a target and biomarker for breast cancer.

Acknowledgments

This work was supported by the National Natural Science Foundation of China (82170431 and 81870259), Natural Science Foundation of Heilongjiang Province (LH2023H012) and Postdoctoral Research Initiation Fund (LBH-Q20152).

Author contributions

Chao Chen: Conceptualization, Writing – review & editing, Writing – original draft, Visualization, Methodology, Investigation, Formal analysis, Data curation. Hongxia Zhang, Lingling Qi, Haoqi Lei, and Xuefei Feng: Investigation, Data curation. Yingjie Chen, Yuanyuan Cheng, and Defeng Pang: Investigation, Formal analysis. Jufeng Wan, Haiying Xu and Shifeng Cao: Formal analysis. Baofeng Yang: Funding acquisition, Resources. Yan Zhang: Funding acquisition, Resources, Supervision. Xin Zhao: Conceptualization, Writing – review & editing, Writing – original draft, Visualization, Methodology, Funding acquisition, Formal analysis, Data curation.

Conflicts of interest

The authors declare no potential conflicts of interest.

Reference

1 Avgerinos KI, Spyrou N, Mantzoros CS, Dalamaga M. Obesity and cancer risk: emerging biological mechanisms and perspectives. *Metabolism* 2019;**92**:121-35.

2 Parra-Soto S, Cowley ES, Rezende LFM, Ferreccio C, Mathers JC, Pell JP, et al. Associations of six adiposity-related markers with incidence and mortality from 24 cancers-findings from the UK Biobank prospective cohort study. *BMC Med* 2021;**19**:7.

3 Ewertz M, Jensen M, Gunnarsdóttir K, Højris I, Jakobsen E, Nielsen D, et al. Effect of obesity on prognosis after early-stage breast cancer. *J Clin Oncol* 2011;**29**:25-31.

4 Fournier F, Diaz-Marin R, Pilon F, Neault M, Juneau R, Girouard G, et al. Obesity triggers tumoral senescence and renders poorly immunogenic malignancies amenable to senolysis. *Proc Natl Acad Sci U S A* 2023;**120**:e2209973120.

5 Chen J, Liu X, Zou Y, Gong J, Ge Z, Lin X, et al. A high-fat diet promotes cancer progression by inducing gut microbiota-mediated leucine production and PMN-MDSC differentiation. *Proc Natl Acad Sci U S A* 2024;**121**:e2306776121.

6 Bader JE, Wolf MM, Lupica-Tondo GL, Madden MZ, Reinfeld BI, Arner EN, et al. Obesity induces PD-1 on macrophages to suppress anti-tumour immunity. *Nature* 2024;**630**:968-75.

7 Piening A, Ebert E, Gottlieb C, Khojandi N, Kuehm LM, Hoft SG, et al. Obesity-related T cell dysfunction impairs immunosurveillance and increases cancer risk. *Nat Commun* 2024;**15**:2835.

8 Schrimpe-Rutledge AC, Codreanu SG, Sherrod SD, McLean JA. Untargeted metabolomics strategies—challenges and emerging directions. *J Am Soc Mass Spectrom* 2016;**27**:1897-905.

9 Johnson CH, Ivanisevic J, Siuzdak G. Metabolomics: beyond biomarkers and towards mechanisms. *Nat Rev Mol Cell Biol* 2016;**17**:451-9.

10 Notarangelo G, Spinelli JB, Perez EM, Baker GJ, Kurmi K, Elia I, et al. Oncometabolite d-2HG alters T cell metabolism to impair $CD8^+$ T cell function. *Science* 2022;**377**:1519-29.

11 Chen C, Zhang Z, Liu C, Sun P, Liu P, Li X. ABCG2 is an itaconate exporter that limits antibacterial innate immunity by alleviating TFEB-dependent lysosomal biogenesis. *Cell Metab* 2024;**36**:498-510.e11.

12 Li J, Zheng C, Mai Q, Huang X, Pan W, Lu J, et al. Tyrosine catabolism enhances genotoxic chemotherapy by suppressing translesion DNA synthesis in epithelial ovarian cancer. *Cell Metab* 2023;**35**:2044-59.e8.

13 Cao T, Zhang W, Wang Q, Wang C, Ma W, Zhang C, et al. Cancer SLC6A6-mediated taurine uptake transactivates immune checkpoint genes and induces exhaustion in $CD8^+$ T cells. *Cell* 2024;**187**:2288-304.e27.

14 Dmitrieva-Posocco O, Wong AC, Lundgren P, Golos AM, Descamps HC, Dohnalová L, et al. β-Hydroxybutyrate suppresses colorectal cancer. *Nature* 2022;**605**:160-5.

15 Gomes AP, Ilter D, Low V, Endress JE, Fernández-García J, Rosenzweig A, et al. Age-induced accumulation of methylmalonic acid promotes tumour progression. *Nature* 2020;**585**:283-7.

16 Fujiwara N, Nakagawa H, Enooku K, Kudo Y, Hayata Y, Nakatsuka T, et al. CPT2 downregulation adapts HCC to lipid-rich environment and promotes carcinogenesis *via* acylcarnitine accumulation in obesity. *Gut* 2018;**67**:1493-504.

17 Di Gangi IM, Mazza T, Fontana A, Copetti M, Fusilli C, Ippolito A, et al. Metabolomic profile in pancreatic cancer patients: a consensus-based approach to identify highly discriminating metabolites. *Oncotarget* 2016;**7**:5815-29.

18 Nunez NP, Perkins SN, Smith NC, Berrigan D, Berendes DM, Varticovski L, et al. Obesity accelerates mouse mammary tumor growth in the absence of ovarian hormones. *Nutr Cancer* 2008;**60**:534-41.

19 Goodsell DS, Morris GM, Olson AJ. Automated docking of flexible ligands: applications of

AutoDock. *J Mol Recognit* 1996;**9**:1-5.

20 Halgren T. New method for fast and accurate binding-site identification and analysis. *Chem Biol Drug Des* 2007;**69**:146-8.

21 Vinci M, Box C, Eccles SA. Three-dimensional (3D) tumor spheroid invasion assay. *J Vis Exp* 2015:e52686.

22 Maguire OA, Ackerman SE, Szwed SK, Maganti AV, Marchildon F, Huang X, et al. Creatine-mediated crosstalk between adipocytes and cancer cells regulates obesity-driven breast cancer. *Cell Metab* 2021;**33**:499-512.e6.

23 Ringel AE, Drijvers JM, Baker GJ, Catozzi A, García-Cañaveras JC, Gassaway BM, et al. Obesity shapes metabolism in the tumor microenvironment to suppress anti-tumor immunity. *Cell* 2020;**183**:1848-66.e26.

24 Bakir B, Chiarella AM, Pitarresi JR, Rustgi AK. EMT, MET, plasticity, and tumor metastasis. *Trends Cell Biol* 2020;**30**:764-76.

25 Dambrova M, Makrecka-Kuka M, Kuka J, Vilskersts R, Nordberg D, Attwood MM, et al. Acylcarnitines: nomenclature, biomarkers, therapeutic potential, drug targets, and clinical trials. *Pharmacol Rev* 2022;**74**:506-51.

26 Riekeberg E, Powers R. New frontiers in metabolomics: from measurement to insight. *F1000Res* 2017;**6**:1148.

27 Ding X, Tian X, Liu W, Li Z. CDHR5 inhibits proliferation of hepatocellular carcinoma and predicts clinical prognosis. *Ir J Med Sci* 2020;**189**:439-47.

28 Hsieh MJ, Chiu TJ, Lin YC, Weng CC, Weng YT, Hsiao CC, et al. Inactivation of APC induces CD34 upregulation to promote epithelial–mesenchymal transition and cancer stem cell traits in pancreatic cancer. *Int J Mol Sci* 2020;**21**:4473.

29 Li J, Diao H, Guan X, Tian X. Kinesin family member C1 (KIFC1) regulated by centrosome protein E (CENPE) promotes proliferation, migration, and epithelial–mesenchymal transition of ovarian cancer. *Med Sci Monit* 2020;**26**:e927869.

30 Sekino Y, Oue N, Shigematsu Y, Ishikawa A, Sakamoto N, Sentani K, et al. KIFC1 induces resistance to docetaxel and is associated with survival of patients with prostate cancer. *Urol Oncol* 2017;**35**:31.e13-31.e20.

31 Ishikawa A, Fujii H, Fukui T, Kido A, Katsuya N, Sentani K, et al. Expression of kinesin family member C1 in pancreatic ductal adenocarcinoma affects tumor progression and stemness. *Pathol Res Pract* 2023;**241**:154277.

32 Wu J, Mikule K, Wang W, Su N, Petteruti P, Gharahdaghi F, et al. Discovery and mechanistic study of a small molecule inhibitor for motor protein KIFC1. *ACS Chem Biol* 2013;**8**:2201-8.

33 Parvin A, Hao SL, Tan FQ, Yang WX. Inhibition of kinesin motor protein KIFC1 by AZ82 induces multipolar mitosis and apoptosis in prostate cancer cell. *Gene* 2020;**760**:144989.

34 Pozdniakova S, Ladilov Y. Functional significance of the adcy10-dependent intracellular cAMP compartments. *J Cardiovasc Dev Dis* 2018;**5**:29.

35 Lomenick B, Hao R, Jonai N, Chin RM, Aghajan M, Warburton S, et al. Target identification using drug affinity responsive target stability (DARTS). *Proc Nat Acad Sci U S A* 2009;**106**:21984-9.

36 Jafari R, Almqvist H, Axelsson H, Ignatushchenko M, Lundbäck T, Nordlund P, et al. The cellular thermal shift assay for evaluating drug target interactions in cells. *Nat Protoc* 2014;**9**:2100-22.

37 Kleinboelting S, Diaz A, Moniot S, van den Heuvel J, Weyand M, Levin LR, et al. Crystal structures of human soluble adenylyl cyclase reveal mechanisms of catalysis and of its activation through

bicarbonate. *Proc Natl Acad Sci U S A* 2014;**111**:3727-32.

38 Zhang H, Kong Q, Wang J, Jiang Y, Hua H. Complex roles of cAMP–PKA–CREB signaling in cancer. *Exp Hematol Oncol* 2020;**9**:32.

39 Fujishita T, Kojima Y, Kajino-Sakamoto R, Mishiro-Sato E, Shimizu Y, Hosoda W, et al. The cAMP/PKA/CREB and TGF*β*/SMAD4 pathways regulate stemness and metastatic potential in colorectal cancer cells. *Cancer Res* 2022;**82**:4179-90.

40 Ramos-Espiritu L, Kleinboelting S, Navarrete FA, Alvau A, Visconti PE, Valsecchi F, et al. Discovery of LRE1 as a specific and allosteric inhibitor of soluble adenylyl cyclase. *Nat Chem Biol* 2016;**12**:838-44.

41 Teng K, Wei S, Zhang C, Chen J, Chen J, Xiao K, et al. KIFC1 is activated by TCF4 and promotes hepatocellular carcinoma pathogenesis by regulating HMGA1 transcriptional activity. *J Exp Clin Cancer Res* 2019;**38**:329.

42 Sepp M, Vihma H, Nurm K, Urb M, Page SC, Roots K, et al. The intellectual disability and schizophrenia associated transcription factor TCF4 is regulated by neuronal activity and protein kinase A. *J Neurosci* 2017;**37**:10516-27.

43 Elagizi A, Kachur S, Carbone S, Lavie CJ, Blair SN. A review of obesity, physical activity, and cardiovascular disease. *Curr Obes Rep* 2020;**9**:571-81.

44 Belladelli F, Montorsi F, Martini A. Metabolic syndrome, obesity and cancer risk. *Curr Opin Urol* 2022;**32**:594-7.

45 Tu H, McQuade JL, Davies MA, Huang M, Xie K, Ye Y, et al. Body mass index and survival after cancer diagnosis: a pan-cancer cohort study of 114 430 patients with cancer. *Innovation (Camb)* 2022;**3**:100344.

46 Du D, Liu C, Qin M, Zhang X, Xi T, Yuan S, et al. Metabolic dysregulation and emerging therapeutical targets for hepatocellular carcinoma. *Acta Pharm Sin B* 2022;**12**:558-80.

47 Wu YY, Gou W, Yan Y, Liu CY, Yang Y, Chen D, et al. Gut microbiota and acylcarnitine metabolites connect the beneficial association between equol and adiposity in adults: a prospective cohort study. *Am J Clin Nutr* 2022;**116**:1831-41.

48 Xiao YX, Yang WX. KIFC1: a promising chemotherapy target for cancer treatment?. *Oncotarget* 2016;**7**:48656-70.

49 Rossetti T, Jackvony S, Buck J, Levin LR. Bicarbonate, carbon dioxide and pH sensing *via* mammalian bicarbonate-regulated soluble adenylyl cyclase. *Interface Focus* 2021;**11**:20200034.

50 Xia L, Oyang L, Lin J, Tan S, Han Y, Wu N, et al. The cancer metabolic reprogramming and immune response. *Mol Cancer* 2021;**20**:28.

Figure captions

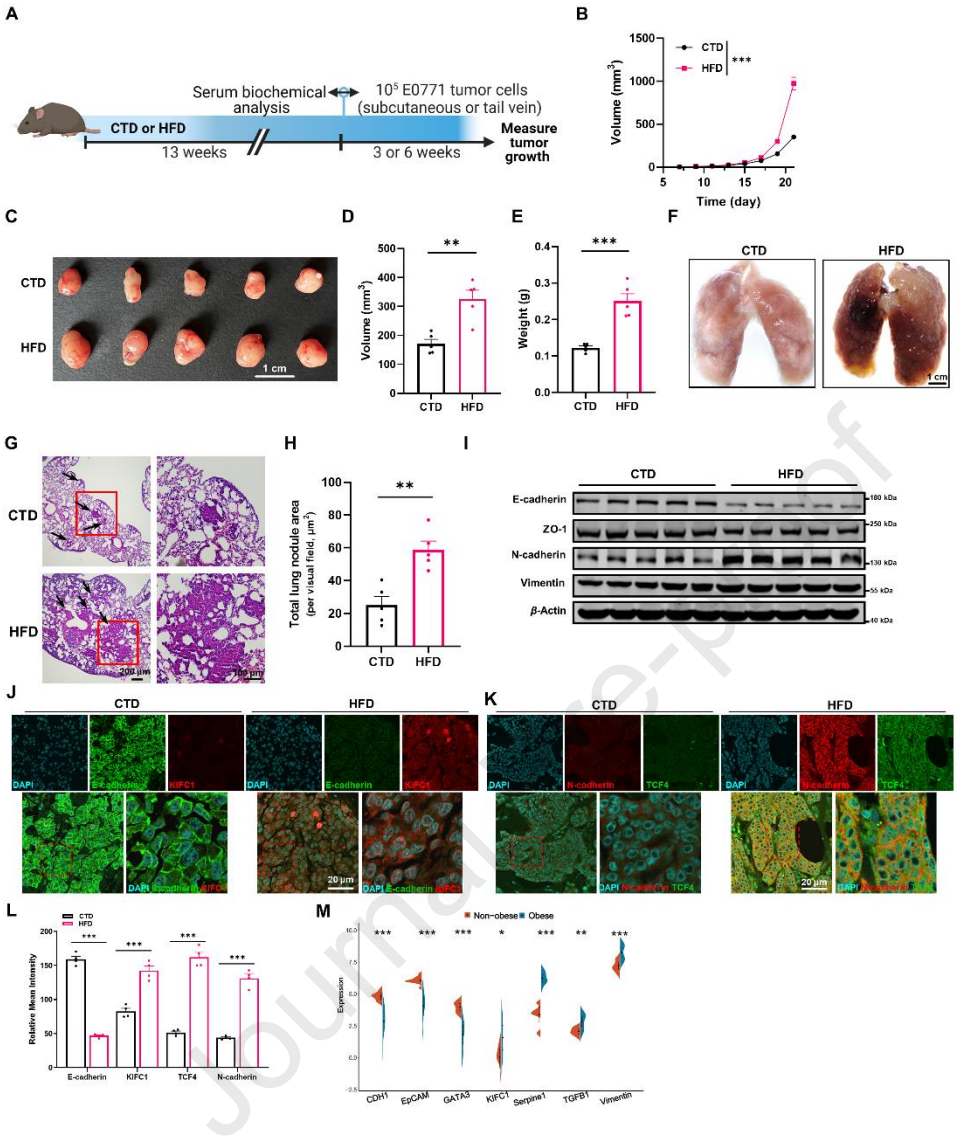

Figure 1 Obesity accelerates breast tumor growth and metastasis. (A) Schematic depicting experimental setup. (B) Tumor growth curves of C57BL/6J mice inoculated with 1×10^5 E0771 tumor cells after CTD or HFD feeding for 13 weeks (*n*=5). (C) Representative pictures of tumors. (D, E) Tumor volumes (D) and weights (E) 21 days after subcutaneous inoculation with E0771 cells in C57BL/6J mice (*n*=5). (F) Pulmonary surface nodules after intravenous injection of E0771 cells in CTD or HFD mice. (G) Representative H&E staining of lung tissues. (H) Quantification of the average number of lung metastatic lesions (*n*=5). (I) Protein levels of EMT markers in tumor tissues derived from CTD or HFD mice (*n*=5). (J–L) Fluorescence intensity represents protein levels of E-cadherin, KIFC1 (J), N-cadherin and TCF4 (K) in tumor tissues derived from CTD or HFD mice. (M) Utilizing the dataset GSE201316, the R packages ggplot and ggpubr were employed to categorize *CDH1*, *EpCAM*, *KIFC1* and other related markers according to obese and non-obese classifications. The Wilcoxon rank-sum test was conducted to evaluate statistical significance

between the groups, with a threshold of $P < 0.05$ denoting statistical significance. For all graphs, unless otherwise specified, the data present mean ± SEM of four independent experiments. Statistical analyses were conducted utilizing Student's *t*-test for B, D, E, H, L and M. $^{**}P < 0.01$, $^{***}P < 0.001$.

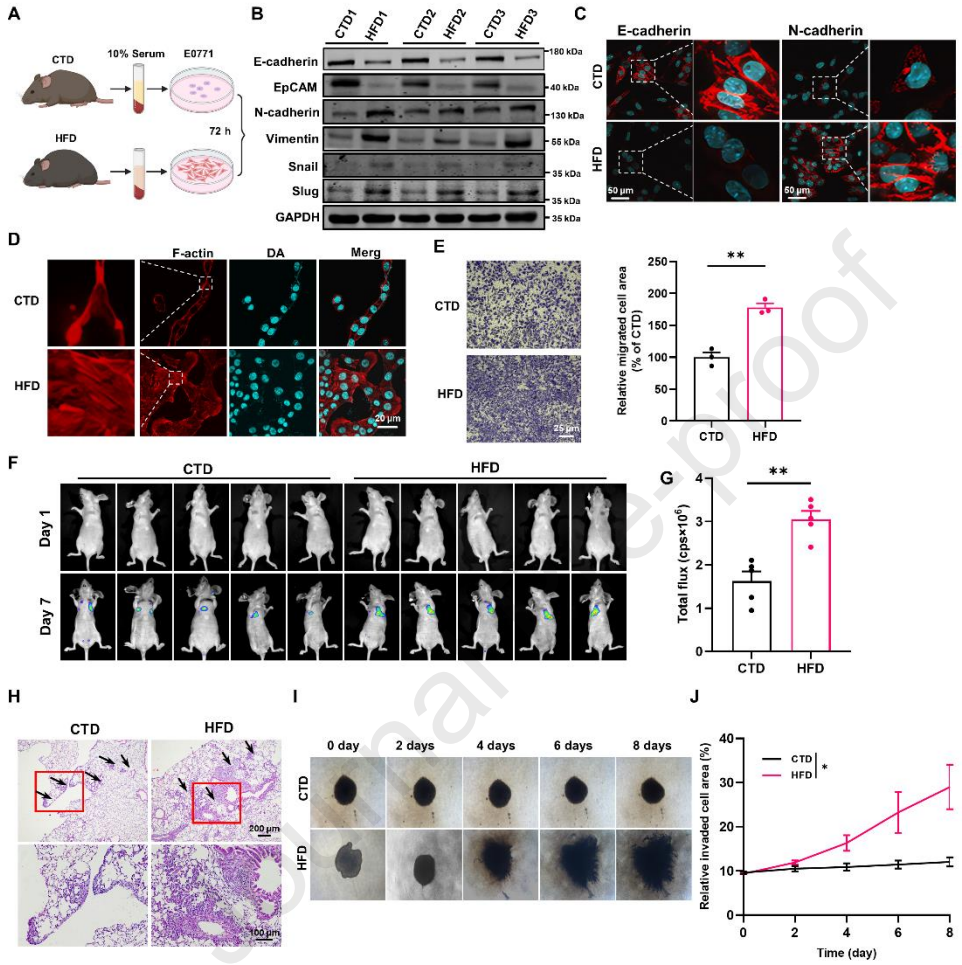

Figure 2 Obesity-induced systemic environment promotes breast cancer aggression. (A) Diagram showing experimental design. (B) Immunoblots of E0771 cells cultured for 3 days in serum from CTD or HFD mice (n=5). (C) Immunofluorescence of E0771 cells cultured for 3 days in serum from CTD or HFD mice; red, E-cadherin or N-cadherin; Cyan, DAPI. (D) Cytoskeleton of E0771 cells cultured for 3 days in serum from CTD or HFD mice. (E) Representative images and quantification of E0771 cells that cultured in transwell plates and treated with serum from CTD or HFD mice after 3 days (n=3). (F, G) Intravenous injection of E0771 cells treated with serum from CTD or HFD mice after 3 days for lung metastasis analysis. Shown are representative images (F) and total flux analyses (G, n=5). (H) Representative H&E staining of lung tissues. (I, J) Representative diagram (I) and quantification (J) of the effect of serum derived from CTD or HFD mice on the invasion of E0771 cells under 3D culture conditions. For all graphs, unless otherwise specified, the data present mean ± SEM of four independent experiments. Statistical analyses were conducted utilizing

Student's *t*-test for E, G, and J. *$P < 0.05$, **$P < 0.01$.

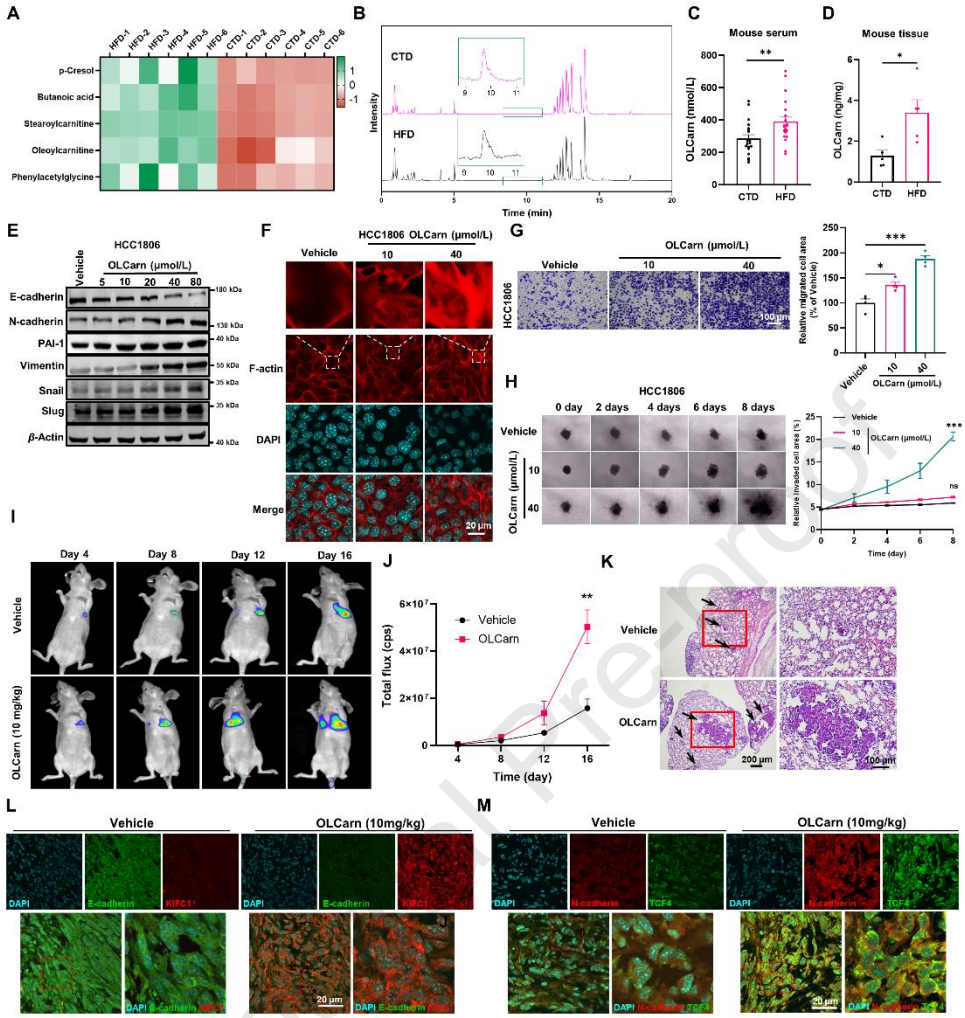

Figure 3 Obese TME derived OLCarn exacerbates breast cancer aggressiveness. (A) Heatmap of 5 metabolites that are increased at a statistically significant level in the serum of HFD mice (*n*=6). (B) Representative HPLC–MS figure depicting the serum composition and OLCarn. (C) Concentrations of OLCarn in all serum samples (*n*=20). (D) Concentrations of OLCarn in all tumor samples (*n*=5). (E) Immunoblots of HCC1806 cells treated with various doses of OLCarn for 3 days; representative images. (F) Cytoskeleton of HCC1806 cells treated with various doses of OLCarn for 3 days; representative images. (G) Transwell migration assays of HCC1806 treated with OLCarn for 3 days. (H) Representative diagram and quantification of the effect of various doses of OLCarn on the invasion of HCC1806 cells under 3D culture conditions. (I, J) Intravenous injection of HCC1806-luciferase cells into nude mice, and subcutaneous injection of OLCarn (10 mg/kg) every 2 days for lung metastasis analysis. Shown are representative images (I) and total flux analyses (J, *n*=5). (K) Representative H&E staining of lung tissues. (L, M) Fluorescence intensity represents protein levels of E-cadherin, KIFC1 (L), N-cadherin and TCF4 (M) in tumor tissues derived from OLCarn treated mice. For all graphs, unless otherwise specified, the data present mean ± SEM of four independent

experiments. Statistical analyses were conducted utilizing Student's *t*-test for C, D and J, one-way ANOVA for G, H.*$P < 0.05$, **$P < 0.01$, ***$P < 0.001$.

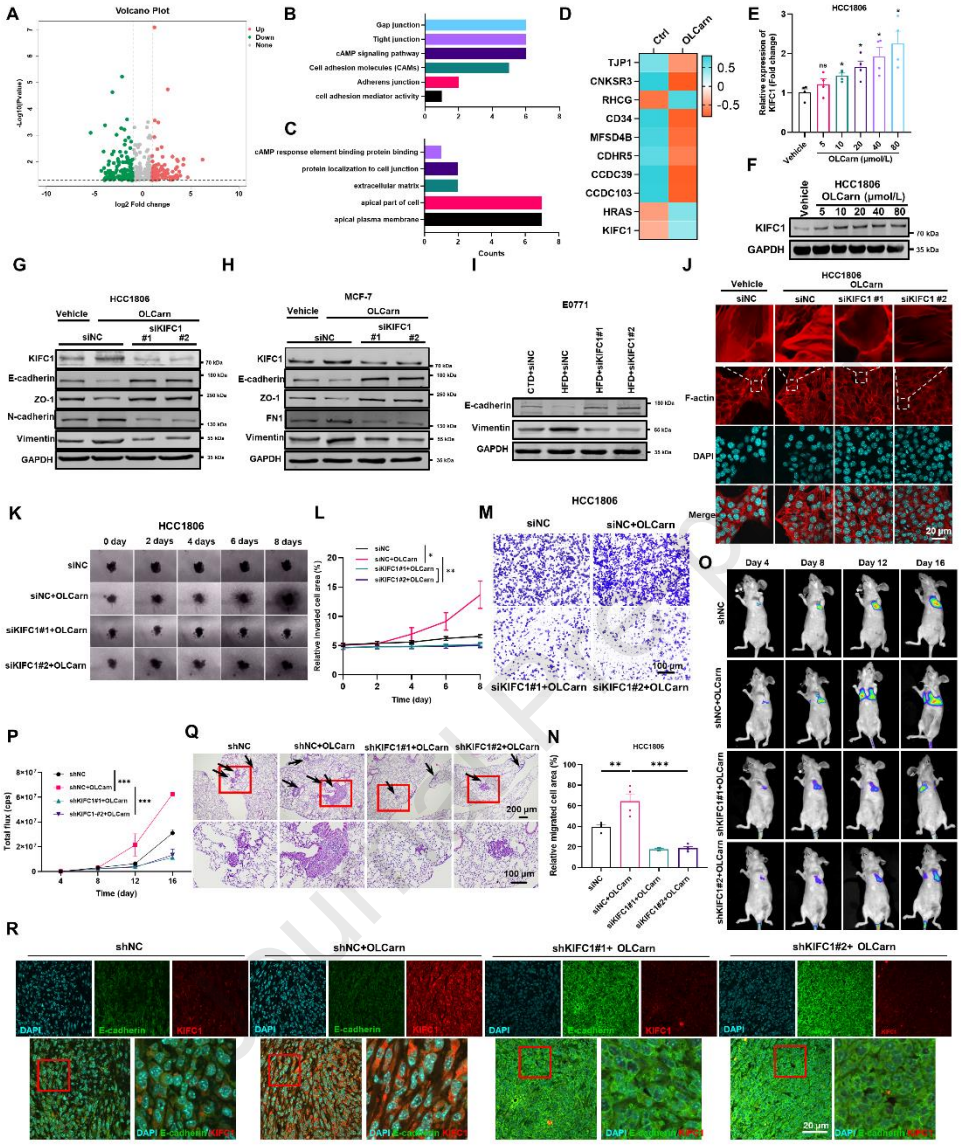

Figure 4 KIFC1 mediates OLCarn-induced pro-aggressive phenotype reprogramming. (A) Volcano map illustrates the comprehensive distribution of differential genes in HCC1806 cells treated with OLCarn for 3 days, wherein red dots symbolize significantly upregulated genes and green dots symbolize downregulated genes. (B, C) GO (B) and KEGG (C) enrichment analysis of differential genes. (D) Heatmap depicting differential genes associated with gap junction and tight junction, etc. (E) mRNA levels of *KIFC1* by RT-PCR in HCC1806 cells treated with various doses of OLCarn for 3 days. (F) Protein levels of KIFC1 by western blot in HCC1806 cells treated with various doses of OLCarn for 3 days. (G, H) Immunoblots of HCC1806 (G) and MCF-7 (H) cells with KIFC1 knockdown and treated with 40 μmol/L OLCarn for 3 days. (I) Immunoblots of E0771 cells with KIFC1 knockdown and treated with serum from CTD or HFD mice for 3 days. (J) Cytoskeleton of

HCC1806 cells with KIFC1 knockdown and treated with 40 μmol/L OLCarn for 3 days. (K, L) 3D invasion assays of HCC1806 cells with KIFC1 knockdown and treated with 40 μmol/L OLCarn for 3 days. (M, N) Transwell invasion assays of HCC1806 cells with KIFC1 knockdown and treated with 40 μmol/L OLCarn for 3 days. (O) Lung colonization assay of HCC1806-luciferase cells with *KIFC1* knockdown (shKIFC1#1 or #2) and treated with 10 mg/kg OLCarn every 2 days (n=5). shNC, non-specific shRNA. (P) The line graph shows the quantification of lung colonization. (Q) Representative H&E staining of lung tissues. (R) Fluorescence intensity represents protein levels of E-cadherin, KIFC1 in tumor tissues derived from mice that KIFC1 knockdown and treated with 10 mg/kg OLCarn every 2 days. For all graphs, unless otherwise specified, the data present mean ± SEM of four independent experiments. Statistical analyses were conducted utilizing one-way ANOVA for E, L, N and P. *$P < 0.05$, **$P < 0.01$, ***$P < 0.001$.

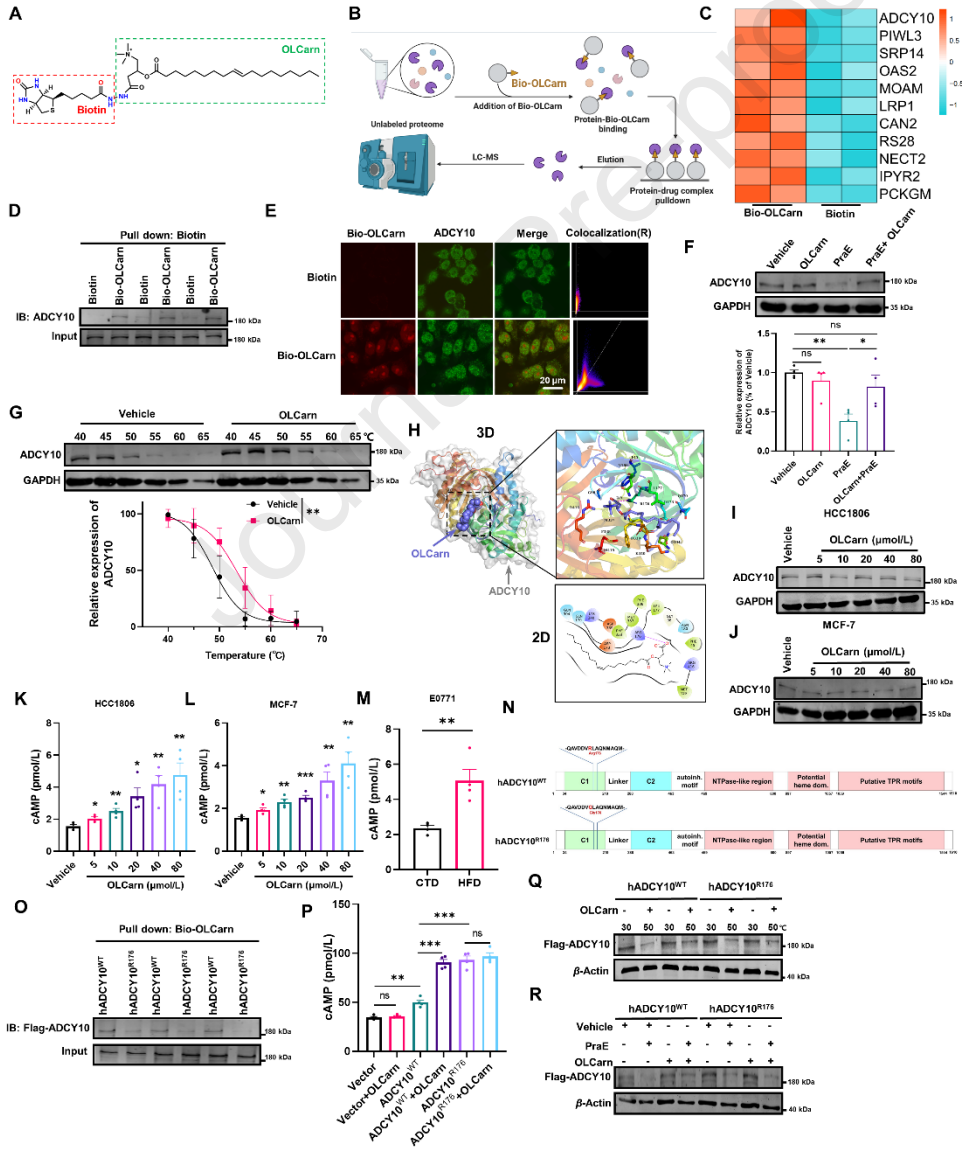

Figure 5 OLCarn directly activating ADCY10 by binding to Arg176 site. (A) The structural formula

of biotin-conjugated OLCarn (Bio-OLCarn). (B) The schematic diagram of streptavidin-biotin affinity pull-down assay. (C) Mass spectrometry analysis identified 11 proteins, including ADCY10, as the cytoplasmic protein from HCC1806 cells pulled down by Bio-OLCarn. (D) Immunoblotting was performed to detect the presence of ADCY10 following co-incubation with cell lysate and subsequent precipitation of bound protein using streptavidin magnetic beads with either Bio-OLCarn or Biotin (20 μmol/L). (E) Fluorescence intensity represents the colocalization of ADCY10 and Bio-OLCarn or biotin (20 μmol/L) in HCC1806 cells; green: ADCY10, red: Bio-OLCarn. (F) Immunoblot analysis of DARTS sample revealed the increased stabilization of ADCY10 during the proteolysis process in HCC1806 cells. (G) OLCarn significantly increased the thermal stability of ADCY10 in CETSA assay at 45–55 ℃ in HCC1806 cells. (H) Computer simulation of OLCarn binding to ADCY 10, and a hydrogen bond was generated between OLCarn and Arg176 on ADCY10. (I, J) Protein levels of ADCY10 by western blot in HCC1806 (I) and MCF-7 (J) cells treated with various doses of OLCarn for 3 days. (K, L) cAMP levels were detected by ELISA in HCC1806 (K) and MCF-7 (L) cells treated with various doses of OLCarn for 3 days. (M) cAMP levels were detected cells by ELISA in E0771 cells treated with serum from CTD or HFD mice for 3 days. (N) Amino acid sequence of the ADCY10 mutation, red: corresponding amino acid sequence. (O) Immunoblotting was conducted to detect the presence of Flag (ADCY10) after co-incubation with cell lysates of $ADCY10^{WT\ or\ R176}$, followed by precipitation of binding proteins using streptavidin magnetic beads and Bio-OLCarn (20 μmol/L). (P) cAMP levels in HEK-293T cells transfected with $ADCY10^{WT\ or\ R176}$ and treated with OLCarn for a duration of 3 days were measured using ELISA. (Q) Immunoblotting analysis of CETSA samples demonstrated the effectiveness of OLCarn in enhancing the thermal stability of wild-type ADCY10 in HEK-293T cells, which was rendered ineffective by the presence of the Arg176 mutation. (R) Immunoblotting analysis of DARTS samples indicated that OLCarn boosted the stability of wild-type ADCY10 during proteolysis in HEK-293T cells, which was nullified by the presence of the Arg^{176} mutation. For all graphs, the data present mean ± SEM of four independent experiments. Statistical analyses were conducted utilizing Student's *t*-test for M, non-linear curve fit for G, one-way ANOVA for F, K, L and P. $*P < 0.05$, $**P < 0.01$, $***P < 0.001$.

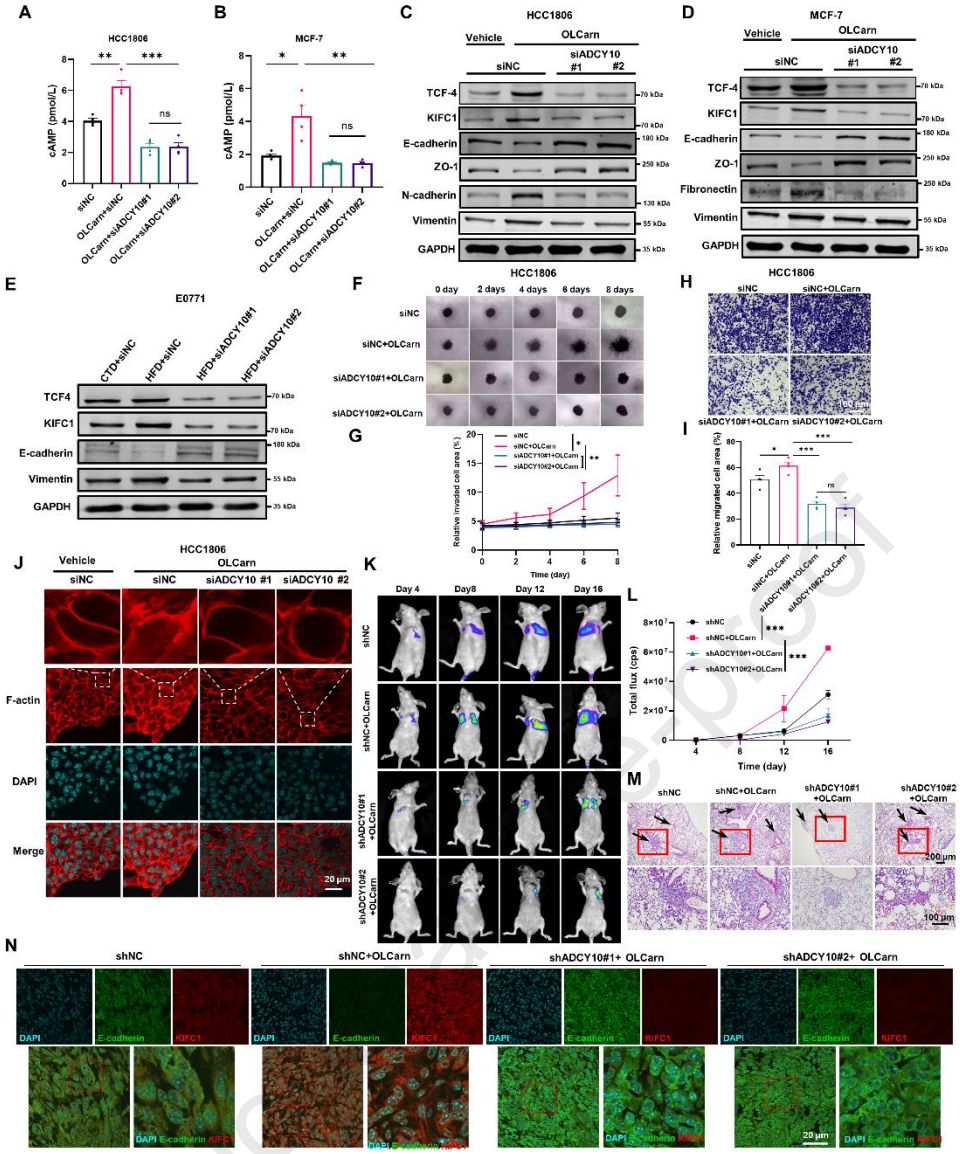

Figure 6 OLCarn induces KIFC1 through activation of ADCY10/cAMP signalling. (A, B) cAMP levels of HCC1806 (A) and MCF-7 cells (B) with ADCY10 knockdown and treated with 40 μmol/L OLCarn for 3 days. (C, D) Immunoblots of HCC1806 (C) and MCF-7 cells (D) with ADCY10 knockdown and treated with 40 μmol/L OLCarn for 3 days. (E) Immunoblots of E0771 cells with ADCY10 knockdown and treated with serum from CTD or HFD mice for 3 days. (F, G) 3D invasion assays of HCC1806 cells with ADCY10 knockdown and treated with 40 μmol/L OLCarn for 3 days. (H, I) Transwell migration assays of HCC1806 cells with ADCY10 knockdown and treated with 40 μmol/L OLCarn for 3 days. (J) Cytoskeleton of HCC1806 cells with ADCY10 knockdown and treated with 40 μmol/L OLCarn for 3 days. (K) Lung colonization assay of HCC1806-luciferase cells with *ADCY10* knockdown (shADCY10#1 or #2) and treated with 10 mg/kg OLCarn every 2 days (n=5). shNC, non-specific shRNA. (L) The line graph shows the quantification of lung colonization. (M) Representative H&E staining of lung tissues. (N) Fluorescence intensity represents protein levels of E-cadherin and KIFC1 in tumor tissues derived from mice that KIFC1

knockdown and treated with 10 mg/kg OLCarn every 2 days. For all graphs, unless otherwise specified, the data present mean ± SEM of four independent experiments. Statistical analyses were conducted utilizing one-way ANOVA for A, B, G, I and L. *$P < 0.05$, **$P < 0.01$, ***$P < 0.001$.

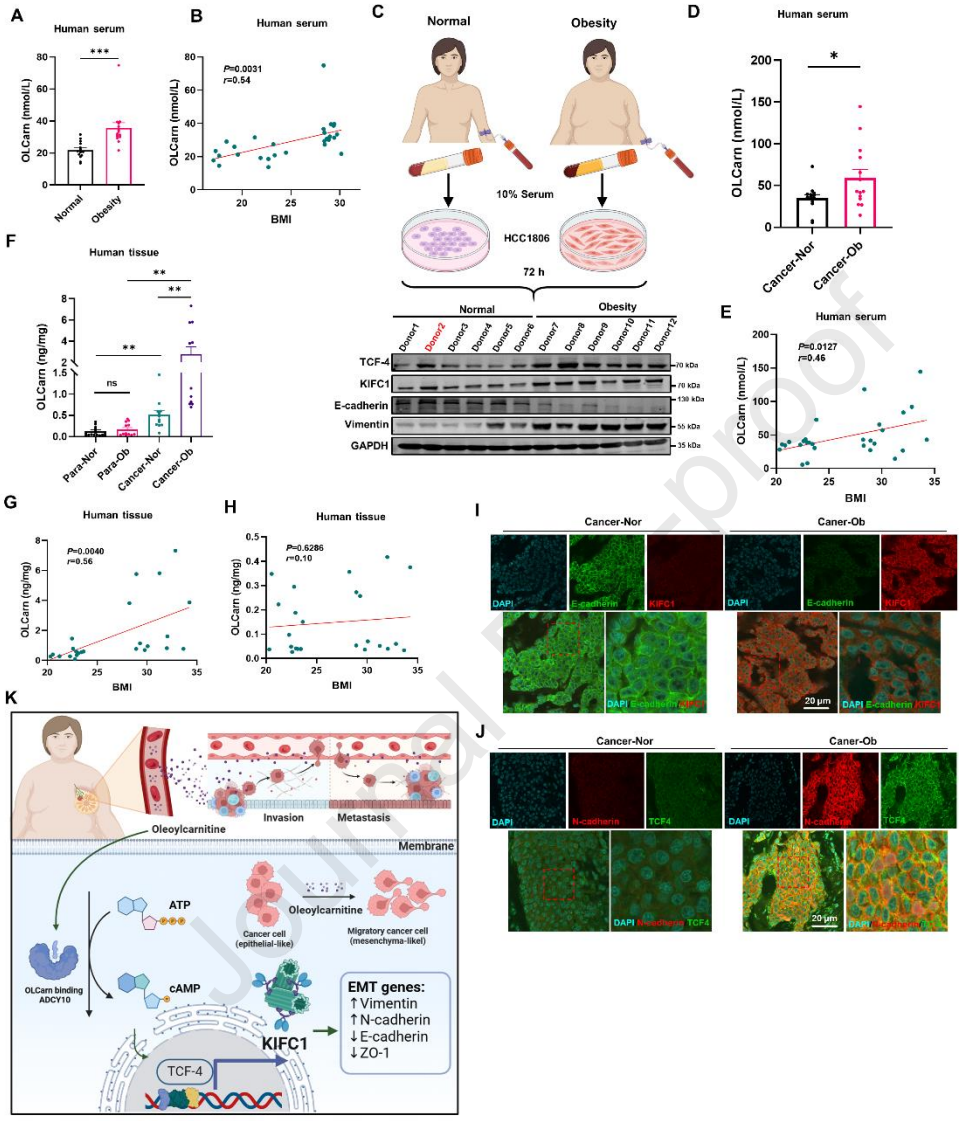

Figure 7 OLCarn correlated with metastatic-like properties as a risk factor for breast cancer. (A) OLCarn concentration in serum samples from individuals without cancer (n=14). (B) BMI was positively correlated with serum OLCarn levels, with a spearman correlation coefficient of 0.54 (n=28). (C) Immunoblots of HCC1806 cells cultured for 3 days in serum from normal weight or obesity donor (n=6). (D) OLCarn concentration in serum samples of breast cancer patients with non-obese or obesity (n=14). (E) BMI was positively correlated with serum levels of OLCarn in breast cancer patients, with a spearman correlation coefficient of 0.46 (n=28). (F) OLCarn concentration in cancer tissue and paracancerous tissue samples of breast cancer patients with normal weight or obesity (n=12). (G) BMI was positively correlated with OLCarn content in

cancerous tissues, with a spearman correlation coefficient of 0.56 (n=24). (H) BMI showed no correlation with OLCarn content in paracancerous tissues. (I, J) Fluorescence intensity represents protein levels of E-cadherin, KIFC1 (I), N-cadherin and TCF4 (J) in tumor tissues derived from breast cancer patients with normal weight or obesity. (K) Schematic representation of the proposed mechanism of OLCarn-induced EMT. Schematic was created with BioRender (www.biorender.com). For all graphs, unless otherwise specified, the data present mean ± SEM of four independent experiments. Statistical analyses were conducted utilizing Student's t-test for A, D, one-way ANOVA for F, Pearson's correlation analysis for B, E, G and H. *$P < 0.05$, **$P < 0.01$, ***$P < 0.001$.

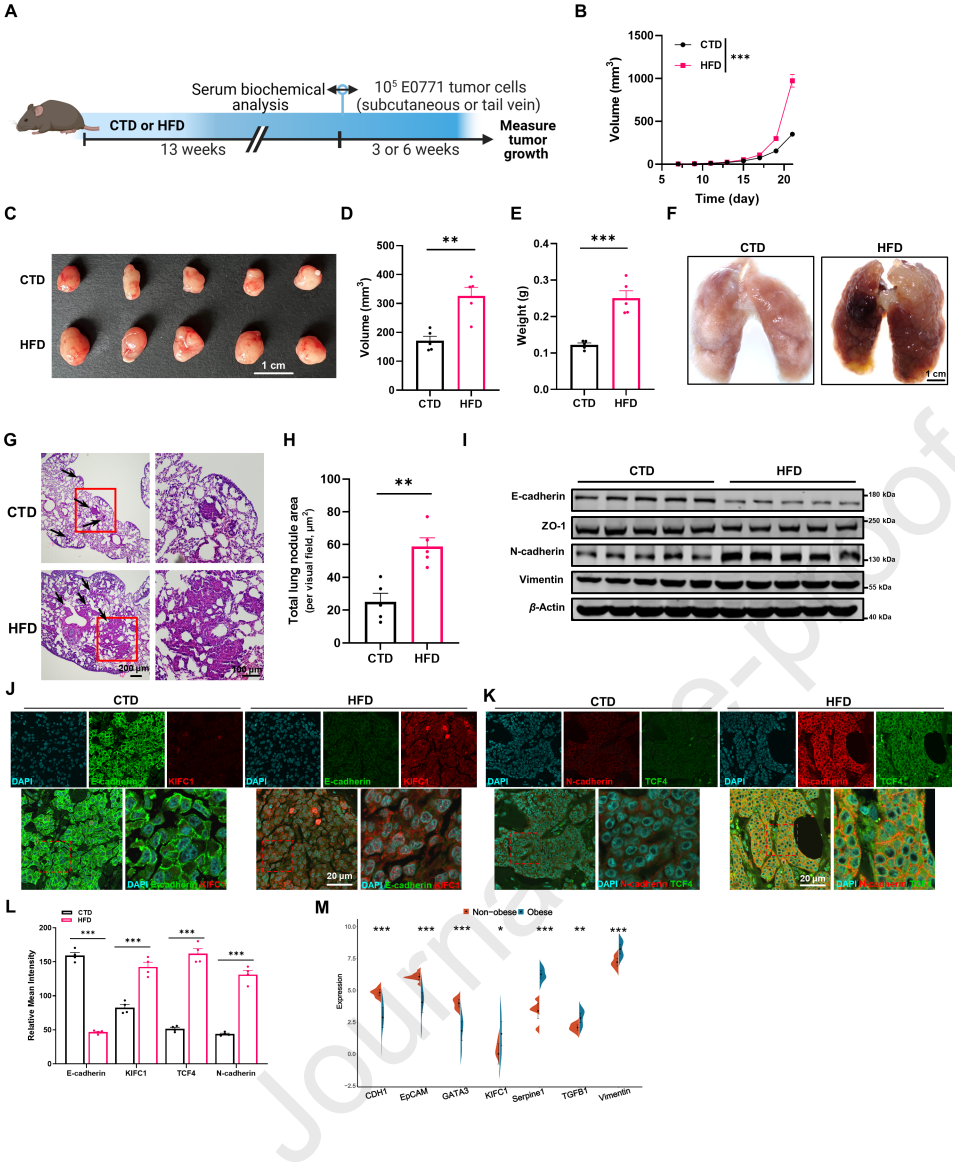

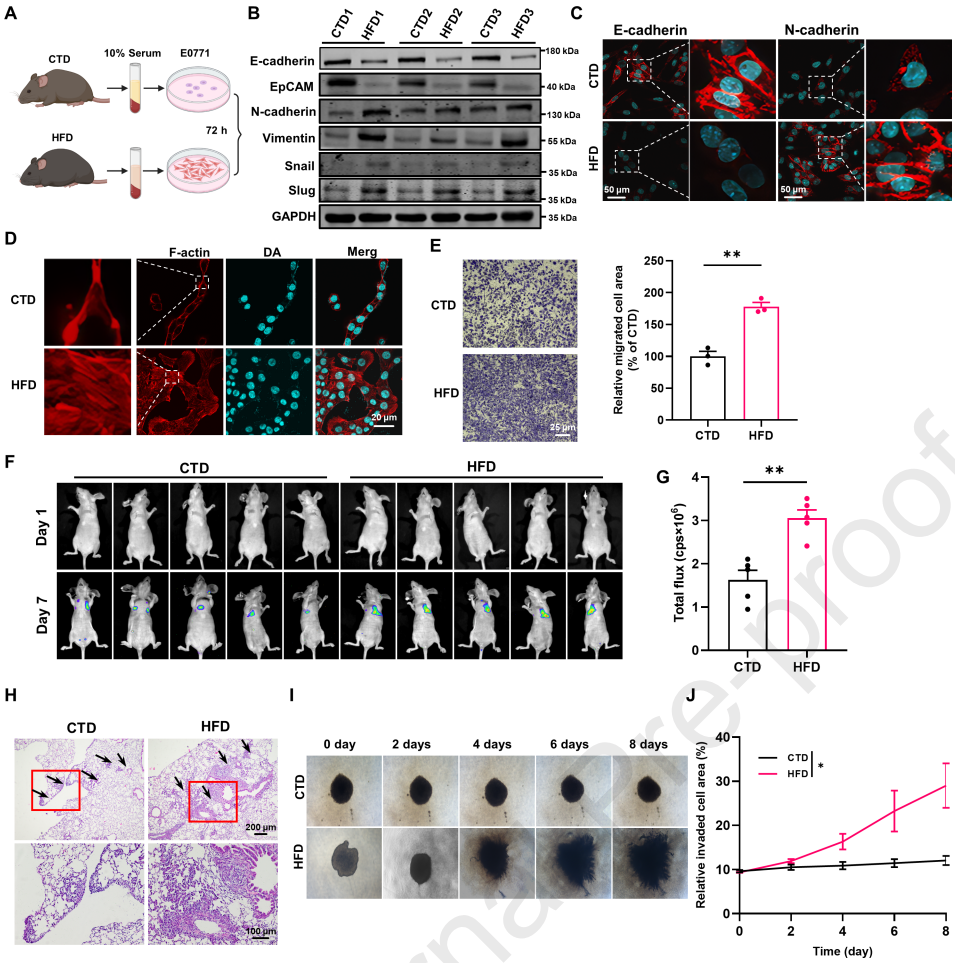

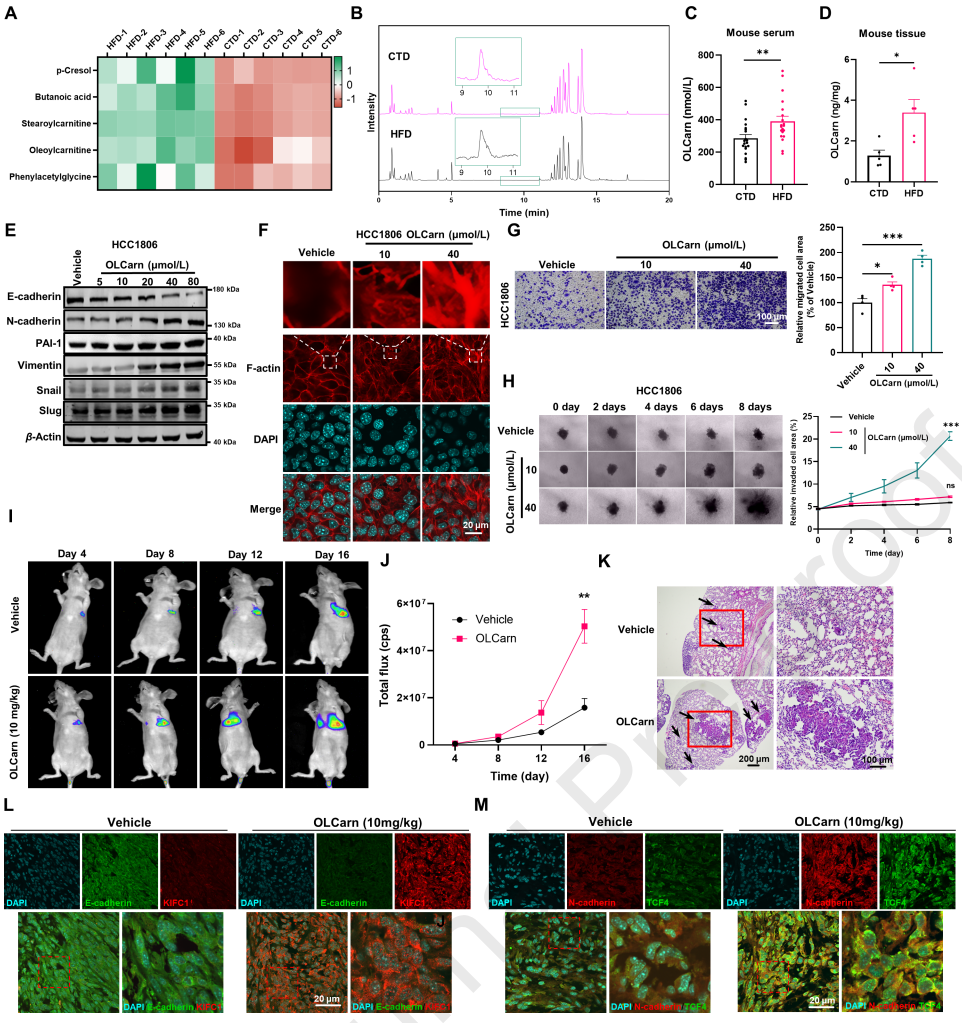

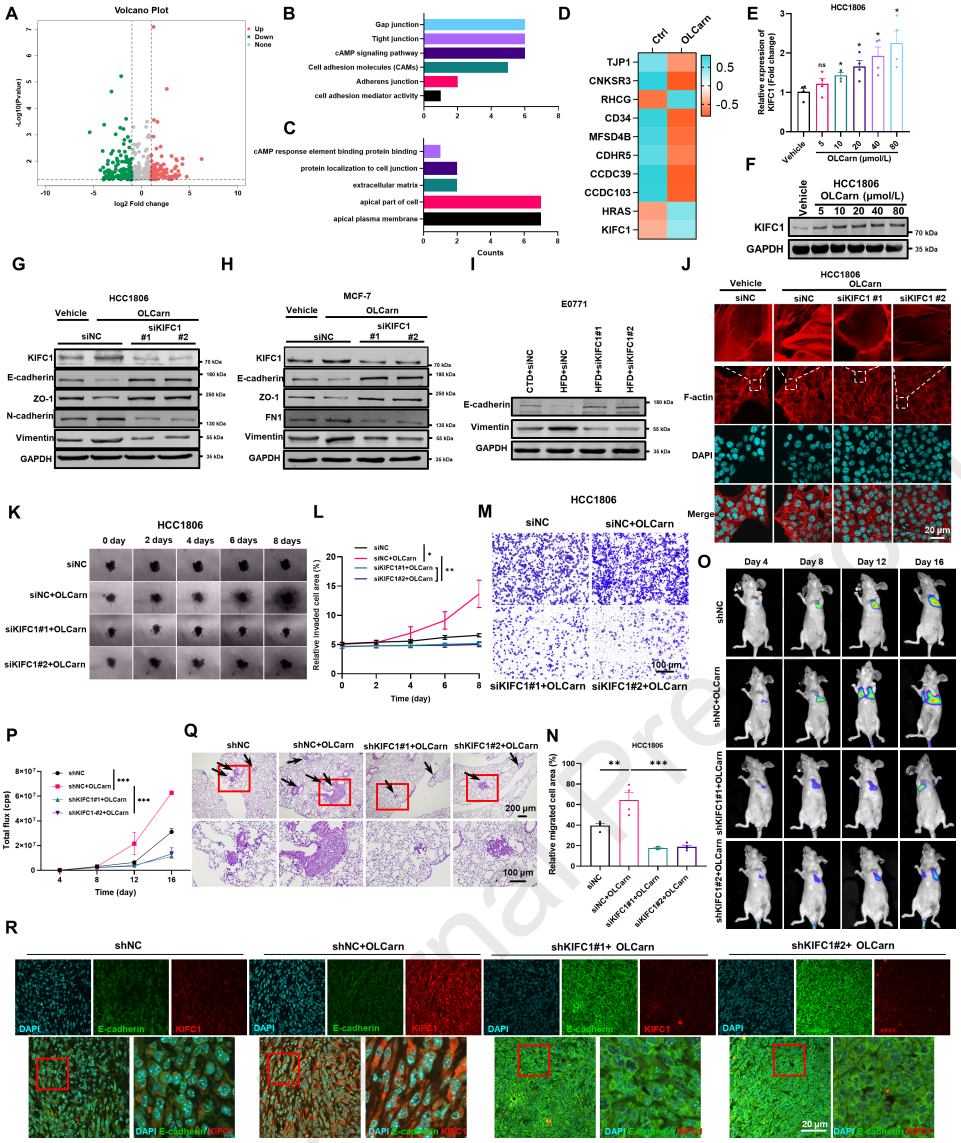
A
Volcano Plot
Up
Down
None
log2 Fold change
B
Gap junction
Tight junction
cAMP signaling pathway
Cell adhesion molecules (CAMs)
Adherens junction
cell adhesion mediator activity
C
cAMP response element binding protein binding
protein localization to cell junction
extracellular matrix
apical part of cell
apical plasma membrane
Counts
D
Ctrl
OLCarn
TJP1
CNKSR3
RHCG
CD34
MFSD4B
CDHR5
CCDC39
CCDC103
HRAS
KIFC1
E
HCC1806
Relative expression of KIFC1 (Fold change)
Vehicle
OLCarn (μmol/L)
F
HCC1806
OLCarn (μmol/L)
KIFC1
GAPDH
G
HCC1806
Vehicle
OLCarn
siNC
siKIFC1 #1
siKIFC1 #2
KIFC1
E-cadherin
ZO-1
N-cadherin
Vimentin
GAPDH
H
MCF-7
I
E0771
CTD+siNC
HFD+siNC
HFD+siKIFC1#1
HFD+siKIFC1#2
J
HCC1806
F-actin
DAPI
Merge
20 μm
K
HCC1806
0 day
2 days
4 days
6 days
8 days
siNC
siNC+OLCarn
siKIFC1#1+OLCarn
siKIFC1#2+OLCarn
L
Relative invaded cell area (%)
Time (day)
M
HCC1806
siNC
siNC+OLCarn
100 μm
O
Day 4
Day 8
Day 12
Day 16
shNC
shNC+OLCarn
shKIFC1#1+OLCarn
shKIFC1#2+OLCarn
P
Total flux (cps)
Time (day)
Q
shNC
shNC+OLCarn
shKIFC1#1+OLCarn
shKIFC1#2+OLCarn
200 μm
100 μm
N
HCC1806
Relative migrated cell area (%)
R
shNC
shNC+OLCarn
shKIFC1#1+ OLCarn
shKIFC1#2+ OLCarn
DAPI
E-cadherin
KIFC1
20 μm

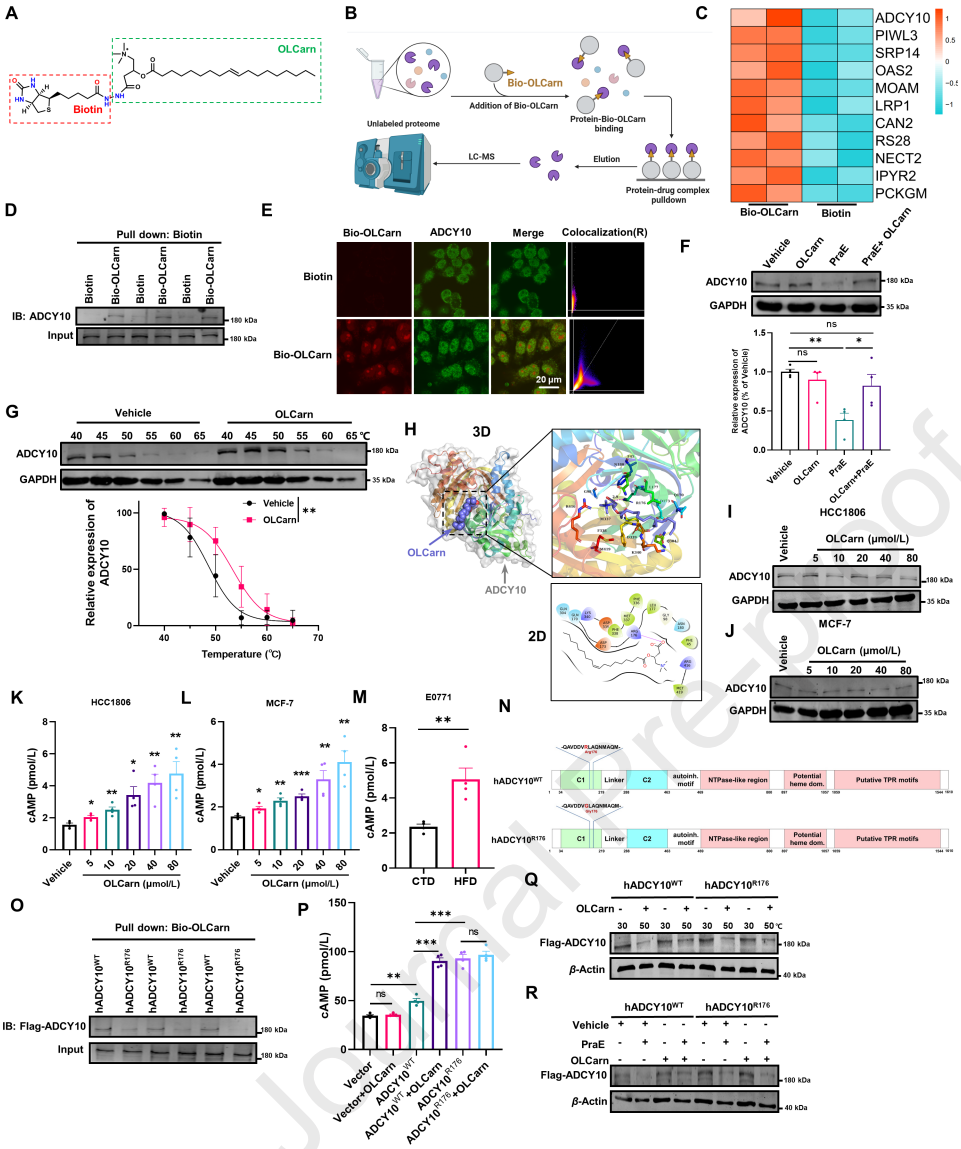

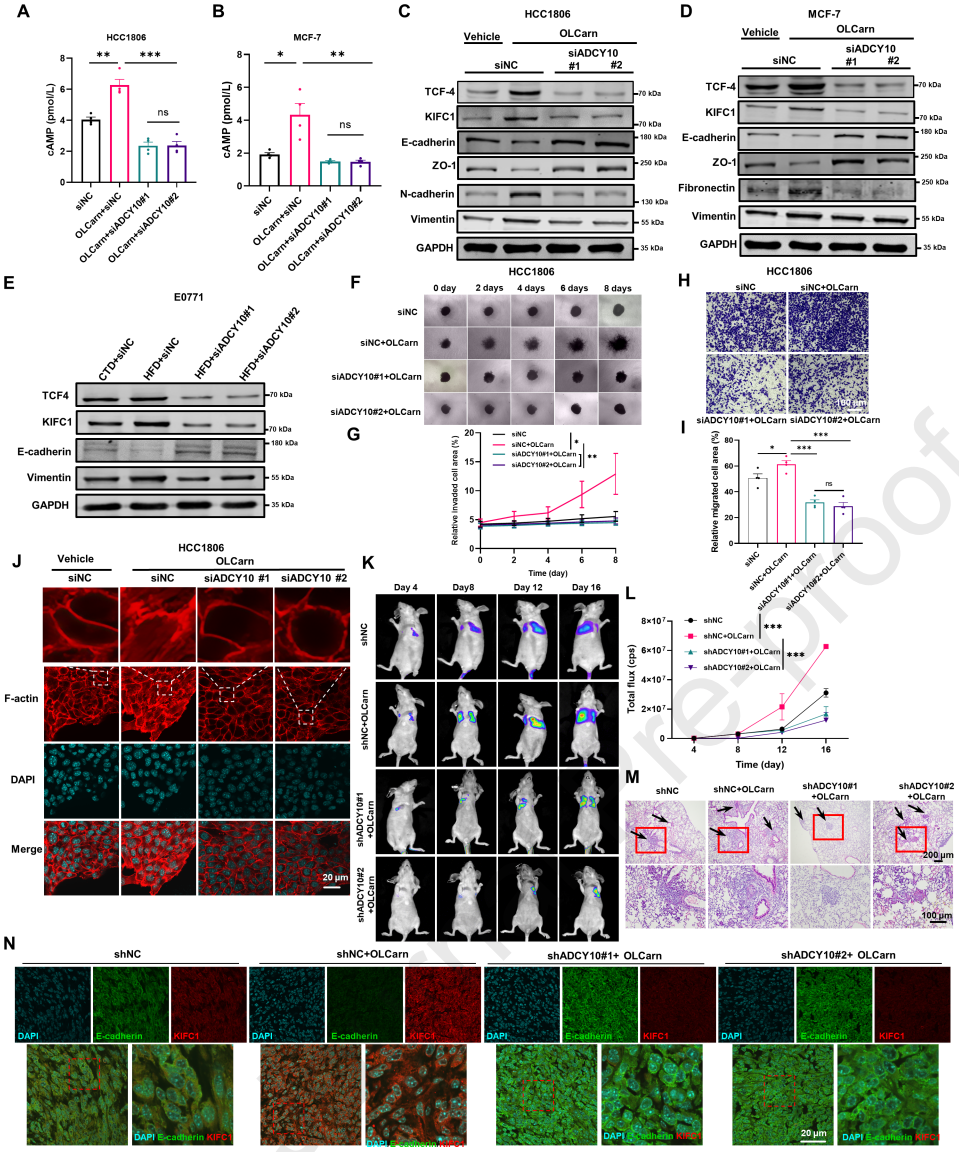

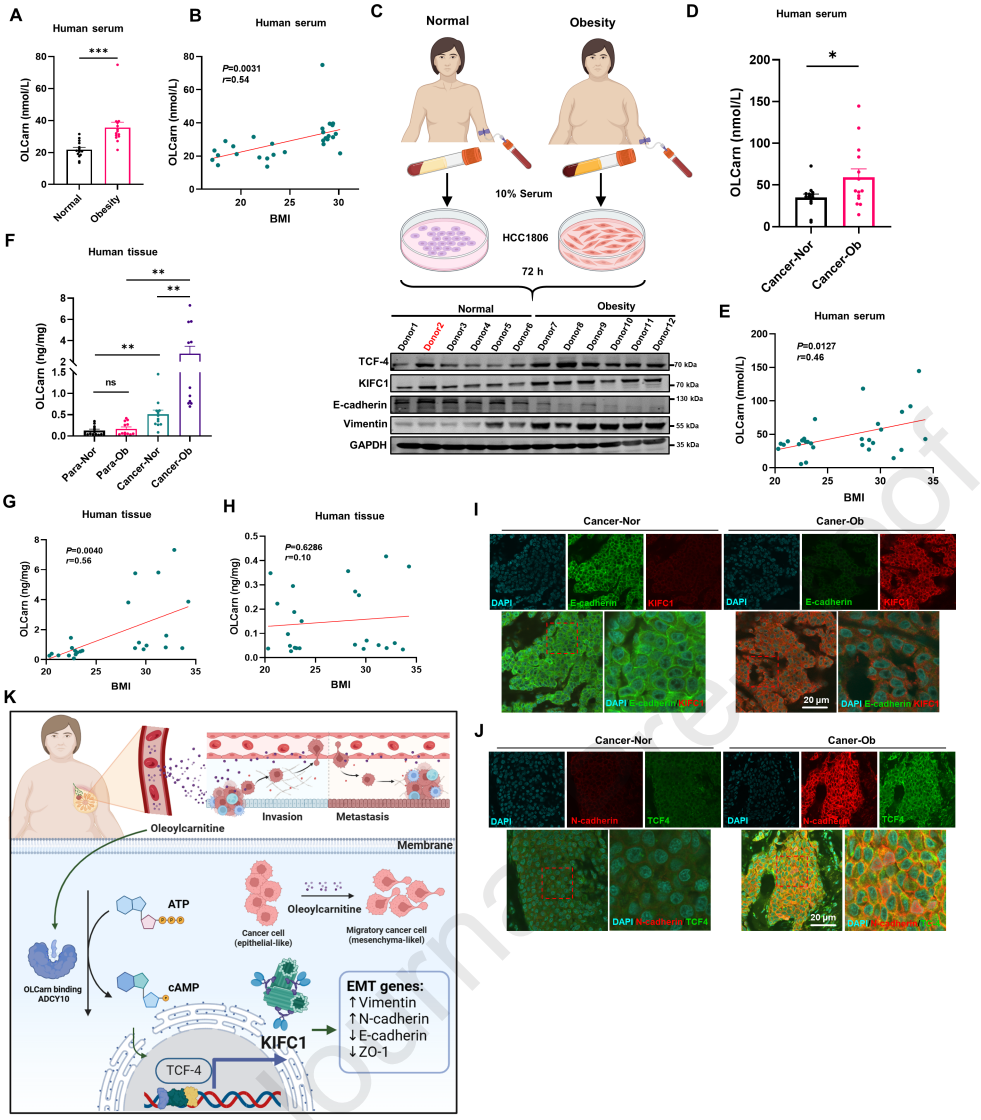
A
Human serum
OLCarn (nmol/L)
Normal
Obesity
B
Human serum
P=0.0031
r=0.54
OLCarn (nmol/L)
BMI
C
Normal
Obesity
10% Serum
HCC1806
72 h
Donor1
Donor2
Donor3
Donor4
Donor5
Donor6
Donor7
Donor8
Donor9
Donor10
Donor11
Donor12
TCF-4
KIFC1
E-cadherin
Vimentin
GAPDH
D
Human serum
OLCarn (nmol/L)
Cancer-Nor
Cancer-Ob
E
Human serum
P=0.0127
r=0.46
OLCarn (nmol/L)
BMI
F
Human tissue
OLCarn (ng/mg)
ns
Para-Nor
Para-Ob
Cancer-Nor
Cancer-Ob
G
Human tissue
P=0.0040
r=0.56
OLCarn (ng/mg)
BMI
H
Human tissue
P=0.6286
r=0.10
OLCarn (ng/mg)
BMI
I
Cancer-Nor
Caner-Ob
DAPI
E-cadherin
KIFC1
20 μm
J
Cancer-Nor
Caner-Ob
DAPI
N-cadherin
TCF4
20 μm
K
Oleoylcarnitine
Invasion
Metastasis
Membrane
ATP
Oleoylcarnitine
Cancer cell (epithelial-like)
Migratory cancer cell (mesenchyma-likel)
OLCarn binding ADCY10
cAMP
KIFC1
TCF-4
EMT genes:
↑Vimentin
↑N-cadherin
↓E-cadherin
↓ZO-1